Impacts of the Madden–Julian Oscillation on Storm-Track Activity, Surface Air Temperature, and Precipitation over North America

CHENG ZHENG, EDMUND KAR-MAN CHANG, HYE-MI KIM, AND MINGHUA ZHANG

School of Marine and Atmospheric Sciences, Stony Brook University, State University of New York, Stony Brook, New York

WANQIU WANG

NOAA/Climate Prediction Center, College Park, Maryland

(Manuscript received 8 August 2017, in final form 9 March 2018)

ABSTRACT

In this study, the intraseasonal variations in storm-track activity, surface air temperature, and precipitation over North America associated with the Madden–Julian oscillation (MJO) in boreal winter (November–April) are investigated. A lag composite strategy that considers different MJO phases and different lag days is developed. The results highlight regions over which the MJO has significant impacts on surface weather on intraseasonal time scales. A north–south shift of storm-track activity associated with the MJO is found over North America. The shift is consistent with the MJO-related surface air temperature anomaly over the eastern United States. In many regions over the western, central, and southeastern United States, the MJO-related precipitation signal is also consistent with nearby storm-track activity. An MJO-related north–south shift of precipitation is also found near the west coast of North America, with the precipitation over California being consistent with the MJO-related storm-track activity over the eastern Pacific. MJO-related temperature and storm-track anomalies are also found near Alaska. Further analyses of streamfunction anomalies and wave activity flux show clear signatures of Rossby wave trains excited by convection anomalies related to MJO phases 3 and 8. These wave trains propagate across the Pacific and North America, bringing an anticyclonic (cyclonic) anomaly to the eastern part of North America, shifting the westerly jet to the north (south), thereby modulating the surface air temperature and storm-track activity over the continent. Rossby waves associated with phases 2 and 6 are also found to impact the U.S. West Coast.

1. Introduction

The Madden–Julian oscillation (MJO), characterized by large-scale eastward-propagating tropical convection, is the dominant mode of intraseasonal tropical variability (Madden and Julian 1971, 1972, 1994). One commonly used index for defining the phase and amplitude of the MJO is the real-time multivariate MJO (RMM) index (Wheeler and Hendon 2004). It separates the MJO as eight different phases depending on the location of MJO convection and associated circulation fields: a positive convective anomaly that develops over the Indian Ocean (phase 1); strengthens and propagates eastward during boreal winter, reaching the eastern Indian Ocean (phases 2–3); the Maritime Continent (phases 4–5); and the western Pacific (phases 6–7). Subsequently this anomaly continues to propagate eastward but weakens, reaching east of the date line by phase 8. The accompanying negative convective anomaly, moves from the Indian Ocean (phase 5), across the eastern Indian Ocean (phases 6–7) and the Maritime Continent (phases 8–1), to the western Pacific (phases 2–3), and reaches east of the date line by phase 4. Many studies (e.g., Hoskins and Karoly 1981; Sardeshmukh and Hoskins 1988; Jin and Hoskins 1995) have shown that tropical diabatic heating source could excite stationary Rossby waves that propagate into the extratropics and significantly modulate the midlatitude circulation. Therefore, the eastward-moving convection associated

Supplemental information related to this paper is available at the Journals Online website: https://doi.org/10.1175/JCLI-D-17-0534.s1.

Corresponding author: Cheng Zheng, cheng.zheng.1@stonybrook.edu

DOI: 10.1175/JCLI-D-17-0534.1

with the MJO can act as diabatic heating source and modify the extratropical circulation (e.g., Matthews et al. 2004; Seo and Son 2012; Riddle et al. 2013). Previous studies have found that the MJO can modulate some important modes of climate variability, such as the North Atlantic Oscillation (NAO; e.g., Cassou 2008; Lin et al. 2009), the Arctic Oscillation (AO; e.g., Zhou and Miller 2005; L'Heureux and Higgins 2008; Flatau and Kim 2013), and the Pacific–North American (PNA) pattern (e.g., Mori and Watanabe 2008; Schreck et al. 2013). Hence, the MJO has an important impact on weather and climate in the midlatitudes.

The MJO can play an important role in modulating surface weather, such as surface air temperature (SAT) and precipitation over North America during winter. Vecchi and Bond (2004) found spatially coherent MJO-related SAT anomalies in high latitudes with amplitudes generally greater than 2°C. Yoo et al. (2011) found that MJO could explain 10%–20% of the SAT trend in Arctic, and changes in the frequency of occurrence of MJO can influence the interdecadal Arctic amplification. Yoo et al. (2012a,b) has shown that Arctic SAT is influenced by MJO-related adiabatic warming/cooling, eddy heat flux, and change in downward infrared radiation. SAT in Canada is also significantly modulated by the MJO (Lin and Brunet 2009), with a warm anomaly in central and eastern Canada 5–15 days after MJO phase 3, and above-normal temperature in northern and northeastern Canada 5–15 days after MJO phase 7. For the United States, Zhou et al. (2012) found significant SAT anomalies in the United States during most of the MJO phases at zero lag, with a very significant warm anomaly in the eastern United States in phases 4, 5, and 6; Schreck et al. (2013) connected these temperature anomalies over the United States with the MJO and the PNA pattern. Baxter et al. (2014) found strong SAT anomalies over the United States from lag composites of MJO phases 3 and 7, and the strongest warm anomaly is in eastern United States 5–20 days after MJO phase 3. Matsueda and Takaya (2015) found that more extreme warm events tend to happen over the eastern part of North America 3–9 days after MJO phases 2–4. Seo et al. (2016) suggested that the MJO influences the midlatitude temperature mainly by horizontal temperature advection.

Furthermore, MJO-related precipitation anomalies have been investigated in many studies. Jones (2000) found that extreme precipitation events in California tend to happen more frequently when the MJO is active, and when the convection is located in the Indian Ocean and decays to the east of the date line as it moves eastward. Donald et al. (2006) found less (more) rainfall over the northern and southern parts of North America and more (less) rainfall in between during MJO phase 4 (phase 8). Bond and Vecchi (2003) found that MJO can significantly modify the precipitation in Oregon and Washington, and the MJO-related wet and dry signals are different during early winter and late winter. Becker et al. (2011) showed a prominent MJO-related cold season precipitation anomaly during MJO phases 5–7 over the central and southern United States, while Zhou et al. (2012) found more MJO-related precipitation over the central United States in phases 5 and 6. The results in Lin et al. (2010) suggested that the precipitation increases significantly after the MJO convection center is over the Indian Ocean, and during the same time, there is also above-normal precipitation in southern Quebec and regions south of the Hudson Bay. The central United States receives more precipitation after phase 3 (Baxter et al. 2014), while Jones and Carvalho (2012) found that extreme precipitation events in the United States are related to MJO phases 3 and 7.

Extratropical cyclones account for much of the high-impact weather in winter, including extreme cold and heavy precipitation events (e.g., Kunkel et al. 2012; Ma and Chang 2017). The aggregate paths over which these cyclones tracks occur are usually referred to as storm tracks. Storm tracks can also be highlighted by maxima in synoptic time-scale variance and covariance statistics (e.g., 500-hPa geopotential height; Blackmon 1976). The MJO can modify the midlatitude storm tracks. Deng and Jiang (2011) found a northeastward-propagating dipole anomaly of a storm track over the Pacific when the convection moves from the eastern Indian Ocean to the west-central Pacific (phases 3–6). Lee and Lim (2012) found a zonal eastward displacement of the Pacific storm-track center during MJO phases 3–6. Grise et al. (2013) suggested that MJO can have an impact on storm tracks over North America during MJO phases 3 and 6. A north–south shift structure of storm-track anomalies has been found in their study, but only the northern part is statistically significant. Guo et al. (2017) performed an investigation of the MJO impact on storm tracks in the entire Northern Hemisphere. A zonal band of strong positive (or negative) storm-track anomalies over 35°–55°N, covering regions from the Pacific, North America, across the Atlantic, and extending toward northern Europe, was found to generally propagate eastward along with the MJO convection.

In most of the recent studies mentioned above, the MJO impact on the extratropics is investigated by either making lag composites within fixed time ranges with respect to one or two MJO phases or compositing with respect to all MJO phases but with no lag. Investigating different MJO phases is important since different phases involve different locations of tropical convection, which

is the source of the Rossby waves. Considering lag relationships is also important since it takes days for the Rossby waves to propagate into the extratropics and reach North America. A method that considers the effects of both different MJO phases and lag days (days after a strong MJO day) is beneficial for a more comprehensive examination of the MJO-related impact on the midlatitudes. In this study, a lag composite strategy with respect to the MJO has been developed to achieve this goal. Furthermore, our strategy allows us to highlight regions over which the MJO impact is important on an intraseasonal time scale. Using this strategy, one can find where the MJO impact is more dominant on one map instead of looking at composite maps of all different MJO phases and different lags.

As discussed above, the MJO can modulate SAT, precipitation, and storm tracks, but these variables are not independent of each other. For example, winter precipitation is mostly brought by storm-track activity. Meanwhile, SAT anomalies can give rise to anomalous temperature gradients that can modify the baroclinicity, giving rise to storm-track anomalies (e.g., Harvey et al. 2014). An interesting question would be whether there is any connection between the MJO impact on these weather variables. Therefore, we will also investigate whether the MJO-related storm-track activity, SAT, and precipitation signals are physically linked with each other, and examine whether these signals can be explained by Rossby wave trains excited by MJO convection.

In section 2, the dataset and methods we use will be introduced. Our lag composite strategy and locations where the MJO-related signal is important locally will be discussed in detail in section 3. In sections 4 and 5, the MJO impact on SAT, precipitation, and storm-track activity over North America and their interconnections will be investigated. Rossby wave trains related to these surface anomalies will be examined in section 6. A summary will be provided in section 7.

2. Data and methods

In this study, similar to previous studies that investigated the MJO impact on storm track (e.g., Grise et al. 2013; Guo et al. 2017), we will focus on the extended boreal winters (November–April) from 1979 to 2016. The 6-hourly mean sea level pressure (MSLP), 2-m SAT, and horizontal wind velocity on pressure levels on a 2.5° × 2.5° horizontal resolution grid are obtained from the European Centre for Medium-Range Weather Forecasts (ECMWF) interim reanalysis (ERA-Interim; Dee et al. 2011). In addition to the reanalysis data, precipitation data over land from the CPC Unified Gauge-Based Analysis of Global Precipitation (Chen et al. 2008) are used to represent daily precipitation over North America on a 0.5° × 0.5° resolution grid. Outgoing longwave radiation (OLR), a variable that is usually used to illustrate the convection in the tropics, is obtained from NOAA interpolated outgoing longwave radiation dataset (Liebmann and Smith 1996).

To quantify storm-track activity, a 24-h difference filter introduced by Wallace et al. (1988) is applied on the MSLP data:

$$\mathrm{pp} = \overline{[p(t + 24\,\mathrm{hr}) - p(t)]^2}. \quad (1)$$

In Eq. (1), p is MSLP, and the 24-h difference is calculated at each time step and on each grid point. Then, pp is computed over a certain time period by averaging the squared MSLP difference. In many previous studies, this averaging is performed over a continuous time (e.g., one month or one season). However, here we apply a similar approach as Guo et al. (2017), in that when making MJO-related composites, the averaging time period does not have to be continuous. As shown by many previous studies (e.g., Lau 1978; Wallace et al. 1988; Chang et al. 2002), the peaks from this 24-h difference filter lie over geographical locations where extratropical cyclones preferentially cross (see also Fig. 1a). Variations in pp will serve as an indicator of storm-track variability.

Various indices have been defined to track the MJO. In this study, we make use of the RMM index, which is a commonly used MJO index. The RMM index is developed based on multivariate empirical orthogonal function (EOF) analysis of combined fields of OLR and 850- and 200-hPa zonal wind anomalies. The first two leading normalized principal components are usually referred to as RMM1 and RMM2. The MJO eight phase life cycle can be defined based on the sign and amplitude of RMM1 and RMM2, and the life cycle is characterized by the eastward propagation of tropical convection from the Indian Ocean toward the Western Hemisphere during boreal winter. In this study, "strong" MJO days are defined as the days when RMM index amplitude is greater than 1 [$(\mathrm{RMM1}^2 + \mathrm{RMM2}^2)^{1/2} \geq 1$]. Only strong MJO days will be used to make the composites. Note that Guo et al. (2017) found that storm-track composites based on an alternative OLR-only index (Kiladis et al. 2014) are very similar to those based on the RMM index.

To test the robustness of our results, two other definitions of strong MJO days (events) have been tested: 1) RMM index amplitude is greater than 1.5; and 2) RMM index amplitude is continuously greater than 1 for at least 25 days, and the MJO has to propagate eastward (phases

in RMM index have to be in the numerical order), and also the MJO cannot stay in one phase for more than 20 days. The latter definition is similar to that in L'Heureux and Higgins (2008) and Riddle et al. (2013). The comparison of the results from the three different strong MJO definitions (not shown) confirms that our results are not sensitive to how strong MJO is defined.

Prior to making the MJO composites, we calculate the daily average values of storm-track activity (i.e., pp) and SAT from 6-hourly data. Then, the local daily climatology, which is the daily mean in 1979–2016, is removed at each grid point from the storm-track activity, SAT, and precipitation data. After that, a 20–100-day bandpass filter, which has a similar frequency with the MJO, is applied to the storm-track activity, SAT, and precipitation field. This bandpass filter will highlight the effect of MJO on these surface weather fields.

To examine Rossby wave trains, we also examine the streamfunction and wave activity flux (WAF) anomalies based on MJO composites. The streamfunction is derived from daily averaged horizontal wind on each pressure level, and the streamfunction anomalies are defined based on daily streamfunction climatology. The definition of WAF is from Takaya and Nakamura (2001) for stationary waves. Under quasigeostrophic assumptions, this WAF is parallel to the local three-dimensional group velocity in a zonal varying basic flow, and the WAF is also independent of the phase of the Rossby wave. The calculation of the WAF requires both streamfunction anomalies and horizontal mean flow. The mean flow used is the average of the whole boreal winter. A sensitivity test performed by calculating WAF with different mean flows (e.g., that correspond to each individual month) shows that using boreal winter mean flow and monthly mean flow yield almost identical results. The streamfunction anomalies and WAF will be applied to examine the Rossby wave train related to the MJO.

3. Lag composite strategy and high MJO impact regions

In this section, we introduce our lag composite strategy that takes into consideration the impact from all eight phases of MJO on up to 30 days after a specific MJO phase. Instead of making pentad composites, or averaging over a few MJO phases, which are performed in many previous studies, our composite strategy will consider the impact of MJO more comprehensively.

An example of our lag composite is shown in Fig. 1. The boreal winter storm-track activity climatology is shown in Fig. 1a. The storm-track activity maxima are over the Pacific and the Atlantic, which are often referred to as the Pacific storm track and the Atlantic storm track. Figure 1b is a composite of anomalous storm-track activity at one grid point with respect to all eight MJO phases and lag days up to 30. The location of the grid point is shown in Fig. 1a. From the lag composite shown in Fig. 1b, the storm-track activity anomaly can be expressed as a function of MJO phases and lag days:

$$\mathrm{pp}'_{\mathrm{MJO}} = \mathrm{pp}'_{\mathrm{MJO}}(\mathrm{phase}_{\mathrm{MJO}}, \mathrm{day}_{\mathrm{lag}}).$$

The prime here means the composited daily anomaly. Then we can calculate $\overline{\mathrm{pp}'^2_{\mathrm{MJO}}}$, which is the mean square of $\mathrm{pp}'_{\mathrm{MJO}}$ over all eight MJO phases and 0–30 lag days. The reason we make a 30-day lag composite is that in many regions to be examined, the statistical significance signal can last up to 30 days. The physical meaning of $\overline{\mathrm{pp}'^2_{\mathrm{MJO}}}$ is the MJO-related variance of storm-track activity from the composite (e.g., Fig. 1b). Large MJO-related variance implies more storm-track variability related to the MJO. So, larger values of $\overline{\mathrm{pp}'^2_{\mathrm{MJO}}}$ mean larger impact from the MJO on storm-track activity in the region.

Lag composites similar to Fig. 1b can be made for each grid point on the map. For each composite, the storm-track activity anomaly $\mathrm{pp}'_{\mathrm{MJO}}$ is also a function of MJO phases and lag days. From these composites, the MJO-related variance $\overline{\mathrm{pp}'^2_{\mathrm{MJO}}}$ can be calculated at each grid point on the map. This is shown in Fig. 2a. It is clear that the MJO-related storm-track variance is large over North Atlantic and North Pacific, which is not surprising as they correspond to the regions where the climatology of storm track is large (Fig. 1a). Also, there is strong MJO-related storm-track variance over Canada. Hence, in terms of variance of storm-track activity in the Northern Hemisphere, MJO has the biggest impact on the North Pacific storm track, the North Atlantic storm track, and central Canada.

The variability of storm-track activity is different from place to place. Therefore, in a place where the intraseasonal variability of the storm track is weak, even if the MJO-related storm-track variability is not large in absolute value compared to North Atlantic or North Pacific, the MJO-induced signal could still be dominant in intraseasonal variability. To further analyze the importance of $\overline{\mathrm{pp}'^2_{\mathrm{MJO}}}$ at each grid box, a Monte Carlo procedure has been applied to test the significance of the $\overline{\mathrm{pp}'^2_{\mathrm{MJO}}}$ signal. The Monte Carlo test takes into account the high autocorrelation in the bandpass-filtered time series by generating 10 000 estimates of composite pp variance from randomly chosen "events" that have the same duration as actual MJO events but with random start dates (details can be found in the appendix). The amplitude of the MJO composite signal can then be

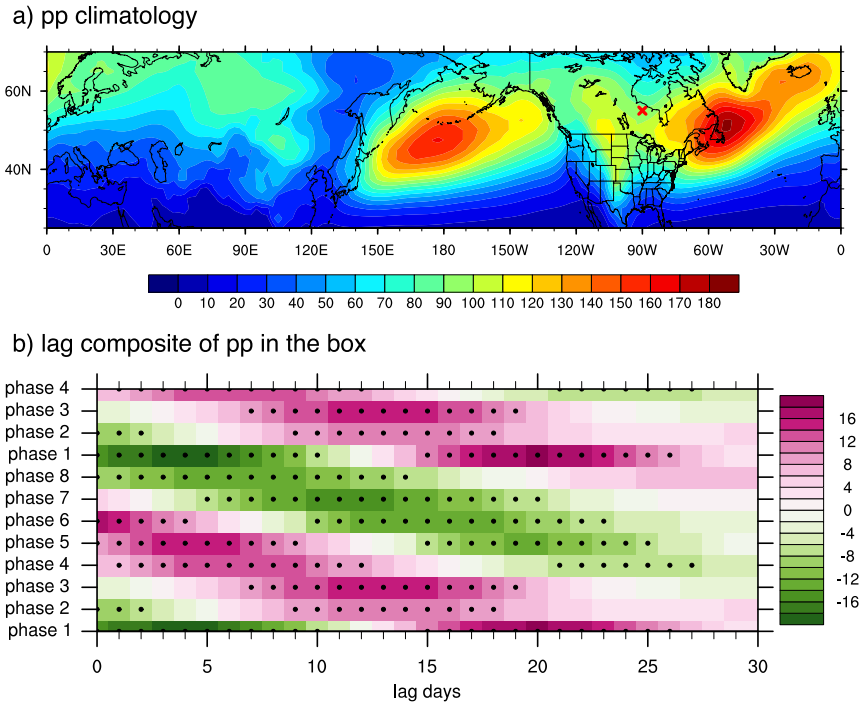

FIG. 1. (a) Climatology of the Northern Hemisphere storm-track activity (pp) during 1979–2016 boreal winters (November–April) based on ERA-Interim data (hPa^2). (b) Lag composite of boreal winter storm-track activity at the grid point located at the red cross (55°N, 90°W) shown in (a), with respect to the eight MJO phases and lag days 0–30 (hPa^2). The dotted boxes are statistically significant at 95% from the results of a Monte Carlo test. An one-and-a-half MJO life cycle is plotted.

compared to those found in the 10 000 random composites to assess statistical significance. In Fig. 2c, the significance level of the composited MJO-related storm-track impact is shown. The subtropical eastern Pacific, the southeastern United States, central Canada, and the southern flank of the North Atlantic storm track, have a significance level that is above 95%. Also, if we consider all the random composites generated by the Monte Carlo procedure as noise, then the mean variance of these random composite will be the mean noise amplitude. The signal-to-noise ratio (Fig. 2b) is the ratio between $\overline{pp'^2_{MJO}}$ and the mean noise amplitude. If the ratio is larger than 1, then the MJO-related storm-track variability is greater than the noise, which is the on-average storm-track variability. From Fig. 2b, we can see that the four regions that have been discussed previously also contain large signal-to-noise ratios. Since this study focuses on the MJO impact on North America, we will not discuss the MJO-related storm-track variability over the eastern Atlantic.

Comparing the three panels of Fig. 2, it is clear that regions where the MJO impact on pp is statistically significant (Fig. 2c) generally have large signal-to-noise ratios (Fig. 2b), but do not necessarily have large MJO-related variances (Fig. 2a). Over regions where the storm track is climatologically weak (e.g., southeastern United States; see Fig. 1a), the signal-to-noise ratio can still be large even if the signal is small (Fig. 2a) because the noise is small. On the other hand, in some regions where the signal is large (e.g., western Atlantic), the noise is so large that the signal-to-noise ratio and statistical significance are small, and the MJO impact, while large, may only account for a small part of the storm-track variations there. In this study, we will focus on regions where the signal-to-noise ratio and statistical significance are high.

The analyses discussed above highlight where the MJO-related storm-track variance is large and where this variance explains a large fraction of local storm-track variability. The same strategy can be applied to examine SAT and precipitation variability associated with the MJO. In Fig. 3a, we can see that MJO is associated with large temperature variability over Alaska, Greenland, Siberia, the eastern United States, and southeastern Canada. The eastern United States and southeastern Canada are the only regions in the midlatitudes to have a large MJO-related temperature variance. Over Alaska, the eastern United States, Greenland, and the western Pacific, the MJO-related temperature variability has large signal-to-noise ratios (Fig. 3b) and is

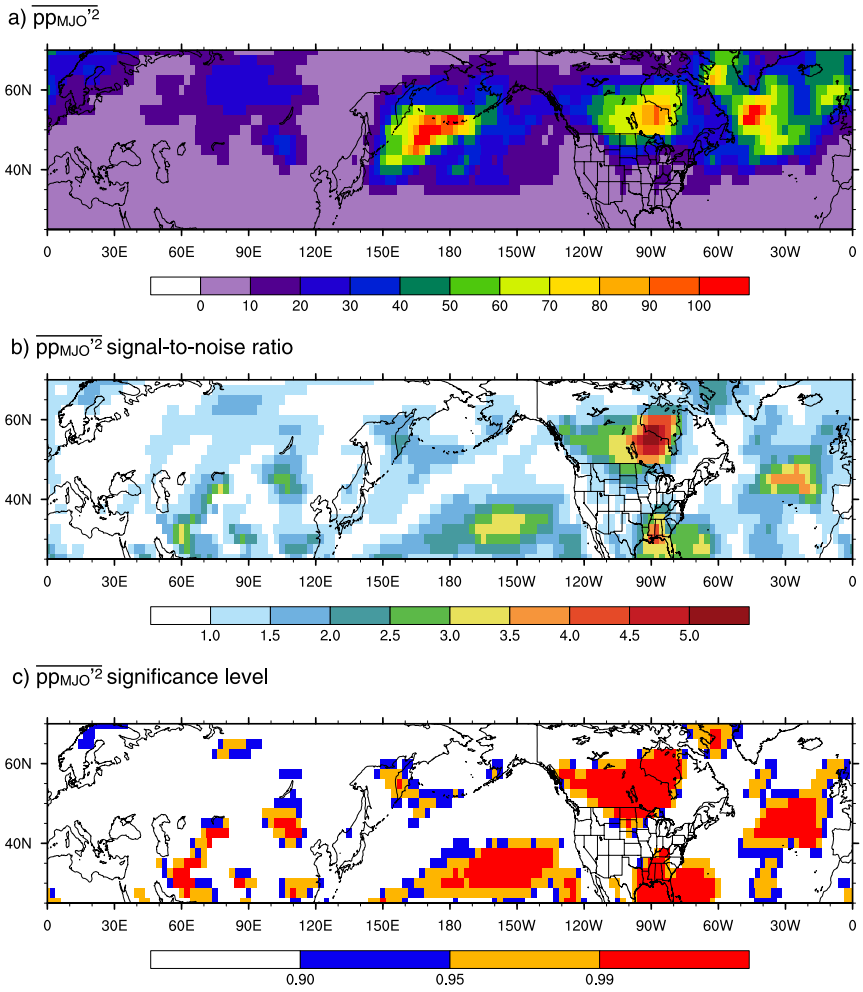

FIG. 2. (a) Mean square of pp'_{MJO} at each grid box. The mean is over all eight MJO phases and 0–30-day lags (hPa^4; see Fig. 1b). (b) Signal-to-noise ratio of $\overline{pp'^2_{MJO}}$, based on a Monte Carlo test (see text for details). (c) The statistical significance level of $\overline{pp'^2_{MJO}}$ at each grid based on a Monte Carlo test.

above the 95% statistical significance level (Fig. 3c). As the magnitude of SAT anomaly is small over the western Pacific (Fig. 3a), the region over the eastern United States and southeastern Canada remains the only region where the MJO impact on SAT is significant (Figs. 3b,c) and large in absolute value (Fig. 3a) in the midlatitudes. Baxter et al. (2014) has shown that, after MJO phase 3, the significant positive SAT anomaly over the eastern United States will appear in a pentad composite up to 25 days, and negative temperature anomaly will cover much of the United States after phase 7; the results in Lin et al. (2009) indicate that warm anomalies appear after MJO phases 2–5 in southeastern Canada, and a large temperature variability appears in the lag composite in northern Canada; the results in Schreck et al. (2013) also indicate that over the eastern United States, there is a large MJO-related temperature anomaly in lag days 6–10. Our results, that through the whole MJO life cycle, SAT has larger variability in the eastern United States, southeastern Canada, and near the Arctic, are consistent with these previous studies.

In Fig. 4a, large MJO-related precipitation variability appears over the west coast of North America and in the southeastern United States. The impact on precipitation is nosier compared to the impact on SAT. One of the reasons is that the precipitation data have higher resolution. Previous studies (Becker et al. 2011; Zhou et al. 2012) have also shown that MJO-related precipitation anomalies are more localized and noisier compared to SAT anomalies. Generally, to have large MJO-related precipitation variability, a region needs to have large climatological precipitation. In regions where winter climatological precipitation is small, even if MJO plays an important role in the precipitation variability, these

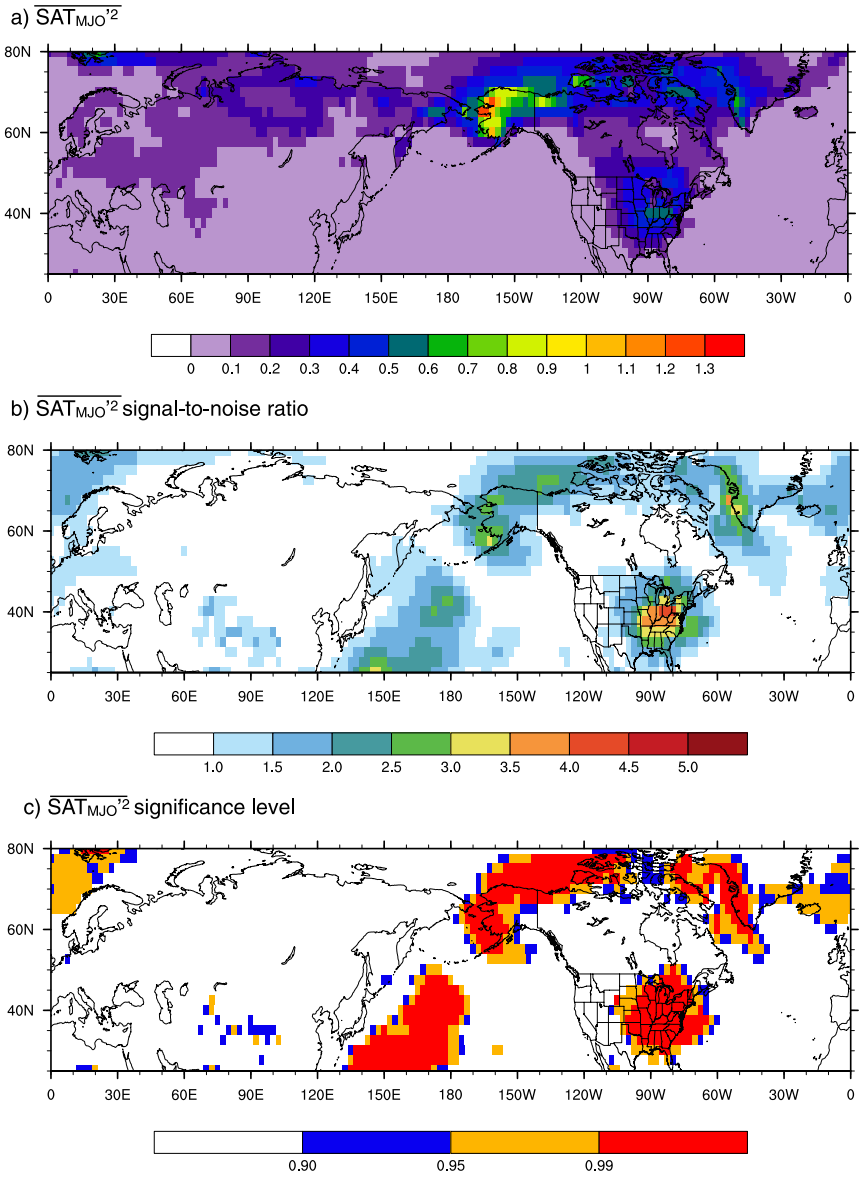

FIG. 3. As in Fig. 2, but for SAT [unit for (a) is K^2].

regions will not show a large value in Fig. 4a. In Fig. 4b, we can see that over British Columbia, Florida, and regions near the Arctic, MJO-related precipitation variability has the highest signal-to-noise ratio. Also, in Fig. 4c, MJO has a statistically significant impact over many regions in North America. Compared to SAT and storm-track activity, the regions where MJO-related precipitation variability is statistically significant are more scattered. We will discuss MJO-related precipitation variability in detail in section 5.

We have shown in this section where MJO has a statistically significant impact on storm-track activity, SAT, and precipitation over North America (Figs. 2c, 3c, and 4c). Consistently, these regions also have a large signal-to-noise ratio (Figs. 2b, 3b, and 4b). The MJO-related variability over these regions will be examined further below.

Note that with our method, regions where the MJO has a significant impact only in one or two MJO phases may not appear to be statistical significant or show a large signal-to-noise ratio. The regions on which we will focus in this study are locations where overall the MJO-related signal is significant throughout much of the MJO life cycle.

4. MJO-related storm-track activity anomalies and SAT anomalies

In this section, the MJO-related storm-track variability and SAT variability will be discussed. We will focus on

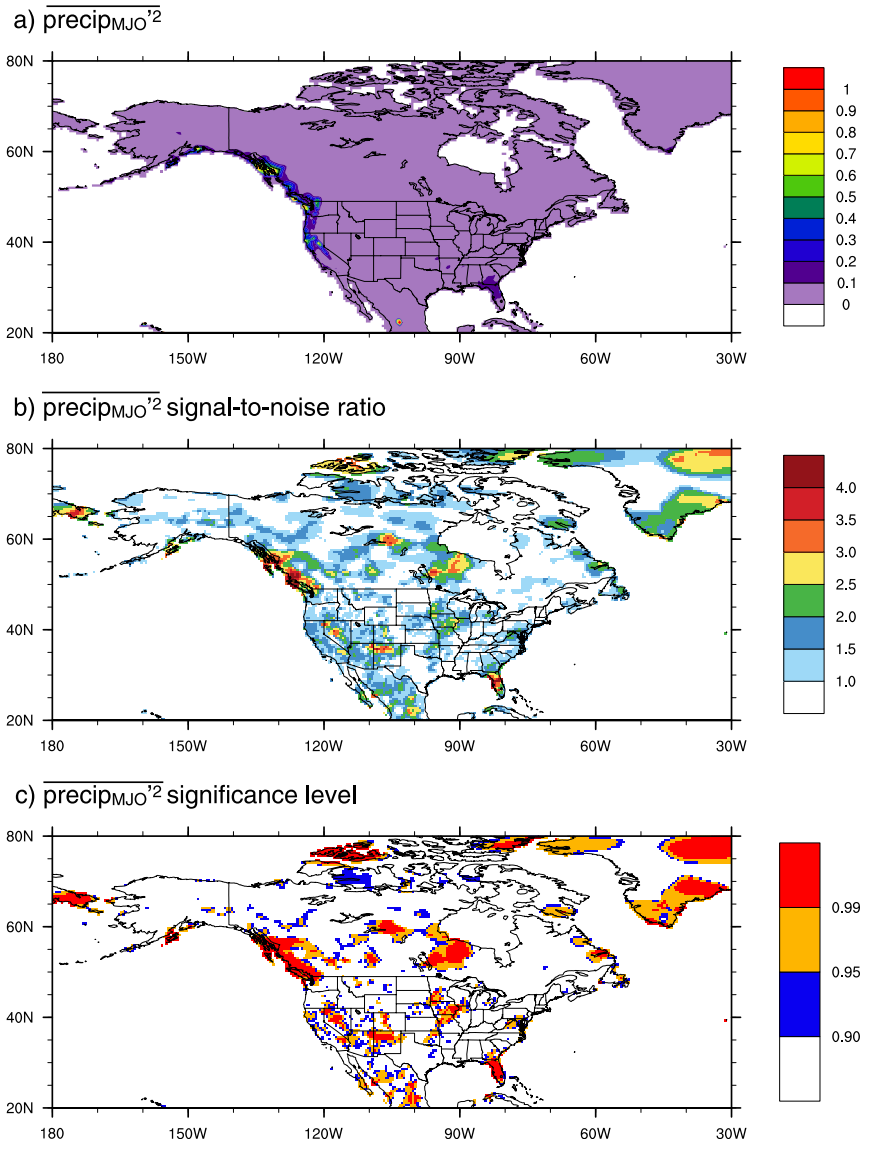

FIG. 4. As in Fig. 2, but for precipitation [unit for (a) is $(\text{mm day}^{-1})^2$].

central Canada (region A) and the southeastern United States (region B) based on the signal-to-noise ratio of MJO-related storm-track variability (Fig. 5a) and significance level (Fig. 5b). Figures 5a and 5b are the same as Figs. 2b and 2c, respectively, but zoomed in for North America.

The lag composite of storm-track activity of region A (Fig. 5e) shows that a statistically significant (95%) positive storm-track activity anomaly appears during lag days 15–25 after MJO phase 1 and extends all the way to lag days 0–4 after phase 6. A significant negative storm-track anomaly appears in region A from lag days 20–28 after phase 4 to lag days 0–3 after phase 2. Positive (or negative) anomalies can usually last continuously for a few MJO phases. The reason is that since each MJO event generally lasts for a few phases, one lag day after a specific phase in this event probably is a day with a smaller lag in the next phase. For a specific MJO phase, the anomaly signal appears about 4–6 days earlier in the next phase. As shown in Wheeler and Hendon (2004), the correlation between RMM1 and RMM2 is at maximum at a lag of 9 days, which indicates the RMM index has a propagation speed of around 4–5 days per phase. Hence, these signals are consistent with the propagation of the MJO from phase 1 to 8 and then back to phase 1. Nevertheless, these composite signals only imply propagation on average, rather than continuous cyclic propagation for any individual event.

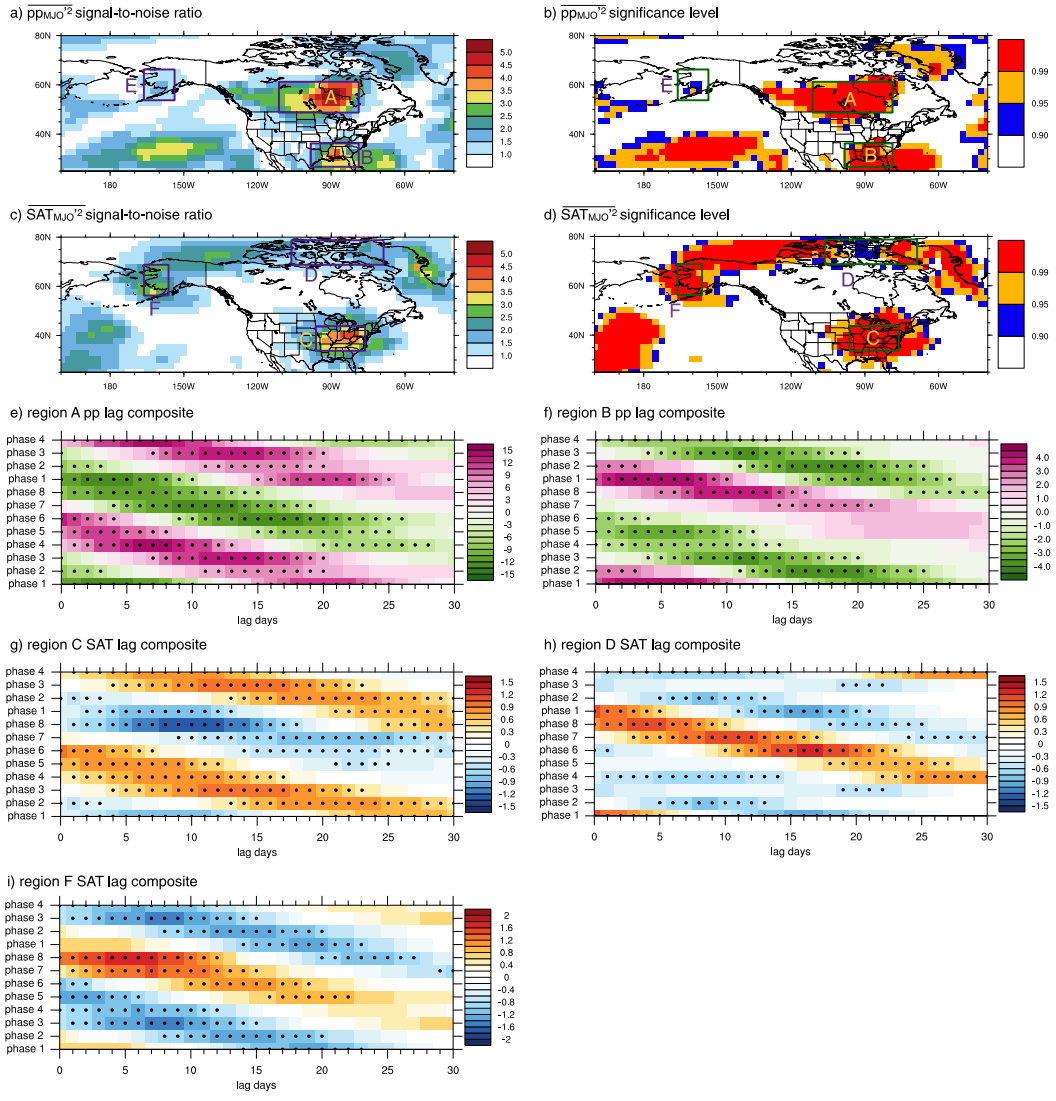

FIG. 5. (a),(b) As in Figs. 2b,c, but focused on the vicinity of North America. (c),(d) As in Figs. 3b,c, but focused on the vicinity of North America. (e) Lag composite of pp anomalies (hPa^2) in region A [48.75°–61.25°N, 111.25°–78.75°W; shown in (a)] with respect to the eight MJO phases and 0–30-day lag. (f) As in (e), but for region B [26.25°–36.25°N, 98.75°–78.75°W; shown in (a)]. (g) Lag composite of SAT anomalies (K) in region C [33.75°–43.75°N, 96.25°–76.25°W; shown in (c)]. (h),(i) As in (g), but for regions D (68.75°–78.75°N, 106.25°–68.75°W) and F (53.75°–66.25°N, 166.25°–156.25°W), respectively [regions shown in (c)]. The dotted boxes in (e)–(i) are statistically significant at the 95% level from the results of a Monte Carlo test.

In region B, from lag days 24–30 after phase 8 to lag days 0–4 after phase 6, there is a negative storm-track anomaly (Fig. 5f); a significant positive storm-track anomaly appears from lag days 14–21 after phase 7 to lag days 0–3 after phase 2. Generally speaking, the anomalies found in corresponding grid boxes in regions A and B have opposite signs. Positive (negative) storm-track activity anomalies in region A are usually associated with negative (positive) anomalies in region B. Therefore, MJO induces a north–south shift of storm-track activity between central Canada and the southeastern United States up to lag day 30.

For the MJO-related SAT anomalies, we first examine the signals over the eastern United States (region C in Fig. 5c) and northern Canada (region D in Fig. 5c). We will mainly focus on region C in this study. Apart from region C, the other regions close to North America where MJO-related variability is important (including region D) are near the Arctic (Fig. 3). Many recent studies have been focused on the MJO-related surface

air temperature anomaly over the Arctic (Yoo et al. 2011, 2012a,b) as discussed in section 1; hence, we will not focus on this region. Here, region D is included only to examine the MJO-related changes in the temperature gradient across central and eastern Canada. Over the eastern United States, significant warm anomalies emerge (Fig. 5g) from days 25–37 (days after lag 30 not shown) after phase 8 to days 0–7 after phase 6; cold anomalies emerge (Fig. 5h) from around day 40 (not shown) after phase 5 to days 0–3 after phase 2. In region D, the SAT signal is generally opposite to that found in region C, but the cold anomaly is not very continuous. The temperature anomaly in region C is consistent with the results of Baxter et al. (2014), Zhou et al. (2012), and Schreck et al. (2013); the anomaly in region D is consistent with the results of Yoo et al. (2011).

Comparing the lag composites of storm-track activity found in regions A and B, and temperature anomalies found in regions C and D (Figs. 5e–h), one can easily find that the anomaly patterns can be divided into two cases. In case 1, when there is a warm anomaly over region C, generally there is a cold anomaly over region D, and at the same time enhanced storm-track activity will appear in region A and the storm-track activity in region B is suppressed. The warm anomaly in region C and cold anomaly in region D implies a stronger meridional temperature gradient over the region between regions C and D. There will also be a weaker temperature gradient south of region C. The temperature anomaly south of region B is statistically significant (not shown). But since compared to the midlatitudes, we do not expect a very large amplitude of MJO-related temperature anomaly in the tropics, the temperature gradient change south of region C is dominated by the temperature change in region C. Generally speaking, we expect stronger storm-track activity to be associated with a stronger temperature gradient. The positive storm-track activity anomaly in region A, which is located between regions C and D, is consistent with the enhanced temperature gradient. The negative storm-track activity anomaly in region B also coincides with the weakened temperature gradient south of region C. In case 2, the anomaly signals of storm-track activity and SAT are generally opposite to case 1 and the signals in regions A, B, C, and D are also consistent with the reversed anomaly patterns. In summary, we find that the MJO can modify the temperature and temperature gradient over North America and induces a north–south shift of storm-track activity, which is consistent with the surface temperature anomaly.

A significant MJO-related SAT anomaly can also be found over Alaska [region F (Fig. 5i); the region is shown in Fig. 5c]. Cold anomalies emerge from days 20–27 after phase 8 to days 0–2 after phase 6; warm anomalies appear from days 16–22 after phase 5 to days 0–12 after phase 8. These anomalies are consistent with the results of Vecchi and Bond (2004) and Yoo et al. (2011). The MJO impact on surface storm-track activity is relatively weak and incoherent near Alaska (region E in Figs. 5a,b, composites not shown). However, the MJO has a significant impact on storm-track activity in the upper troposphere south of Alaska (not shown). This upper-level storm-track activity signal is consistent with the results of Guo et al. (2017), and it may be related to the temperature gradient change associated with the SAT anomaly over region F. As discussed in Guo et al. (2017), upper-level and surface storm-track signals are not always consistent with each other. Further studies will be needed to investigate why this is the case.

5. MJO-related precipitation anomalies

In this section, we will inspect regions where the MJO-related precipitation variability has a large signal-to-noise ratio and high significance (Figs. 6c,d). Since winter precipitation is usually associated with large-scale weather systems, which are mainly extratropical cyclones, we will also examine the connection between the MJO-related winter precipitation anomaly and the MJO-related storm-track variability. The MJO-related precipitation signal is noisy over North America (Fig. 4), but we just use original resolution data to highlight the high-impact region and do the significance analysis. We will focus on the lag composites of precipitation in this section. The lag composites are spatially averaged, so the signal is smoothed. As the statistically significance precipitation signal is scattered and we cannot investigate all of the regions, we just select the regions where the signal-to-noise ratio is big over a large area, and focus more on regions where large population centers lie. Some subjectivity is inevitable when choosing where to place the precipitation boxes over the map. But since most winter precipitation is brought by large-scale weather systems (e.g., extratropical cyclones), nearby precipitation grid points will not have a very different signal. Thus, moving the precipitation box by one or two grid points, or making the box a bit bigger or smaller will not change our composited results much.

In Fig. 6, we investigate the regions along the west coast of North America where MJO has a high impact on storm-track activity and precipitation. Several studies have shown that tropical heating can have a significant impact on winter precipitation (Mo and Higgins 1998; Higgins et al. 2000; Jones 2000) and snowpack (Guan et al. 2012) over the west coast of North America. Chang et al. (2015) has shown that on seasonal time scales, precipitation in California is highly modulated by

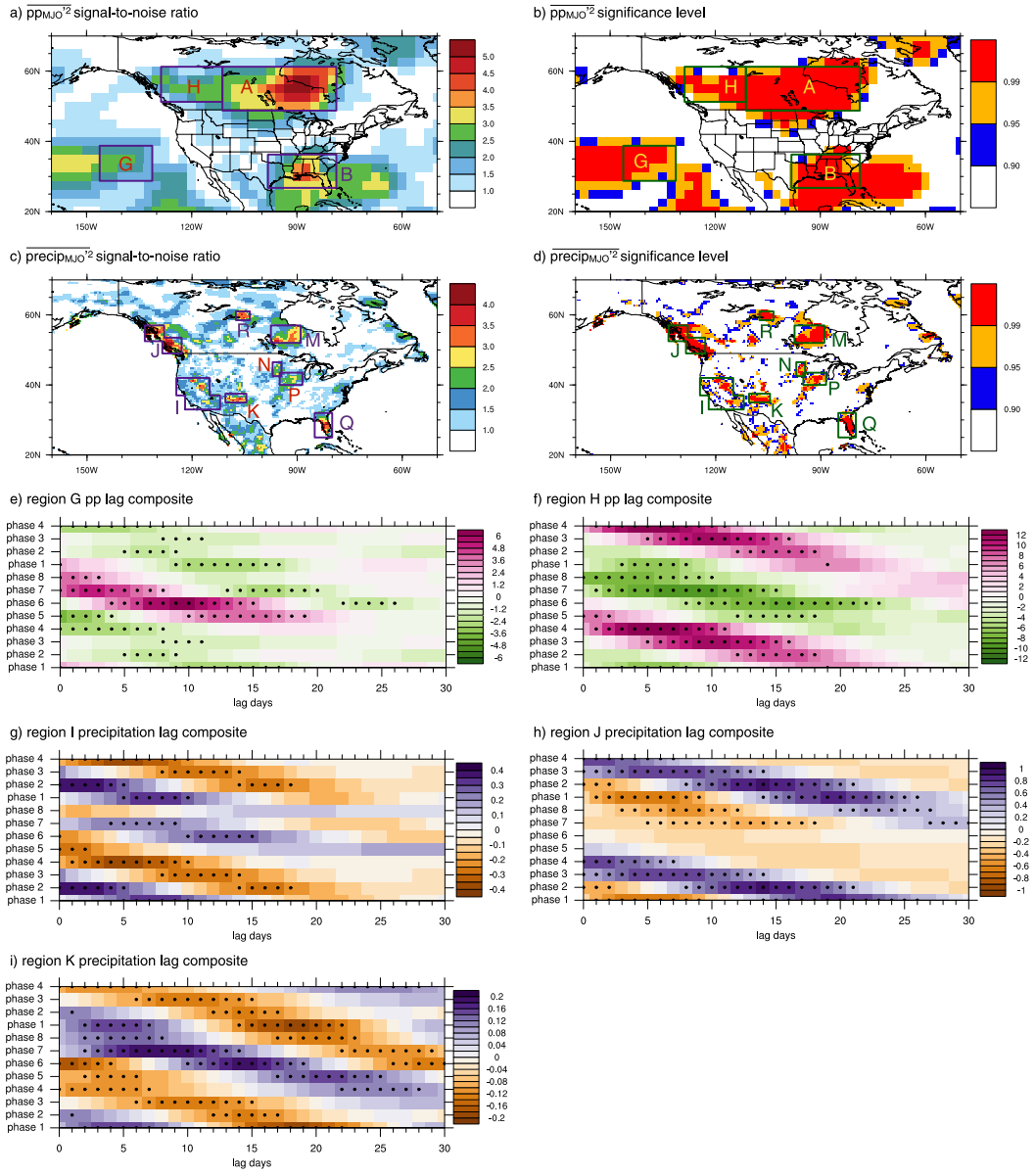

FIG. 6. (a),(b) As in Figs. 2b,c, but focused on the vicinity of North America. (c),(d) As in Figs. 4c,d. (e) Lag composite of pp anomalies (hPa^2) in area G [26.25°–38.75°N, 146.25°–131.25°W; shown in (a)]. (f) As in (e), but for region H [51.25°–61.25°N, 128.75°–111.25°W; shown in (a)]. (g) Lag composite of precipitation anomalies ($mm\ day^{-1}$) in region I [combination of boxes 33.0°–37.0°N, 122.0°–112.0°W and 37.0°–42.0°N, 124.5°–115.0°W; shown in (c)]. (h) As in (g), but for region J [combination of boxes 49.0°–53.5°N, 128.5°–123.0°W and box 52.5°–57.0°N, 133.5°–128.0°W; shown in (c)]. (i) As in (g), but for region K [35.0°–37.5°N, 110.5°–104.5°W; shown in (c)]. The dotted boxes in (e)–(i) are statistically significant at the 95% level from the results of a Monte Carlo test.

storm-track activity over the eastern Pacific (region G). Region G is placed in a location where the MJO has a significant impact on storm-track activity in all of the grid points (Fig. 6b), and the storm-track activity in the region has a high correlation with the precipitation over region I (California and Nevada) on intraseasonal time scales (not shown). Note that moving region G by up to 5° longitude eastward or westward (not shown) barely changes the pattern of the storm-track activity lag composite (Fig. 6e).

In Fig. 6e, significant negative storm-track activity in region G appears from days 11–18 after phase 1 to days 0–3 after phase 5; positive storm-track activity appears from days 10–18 after phase 5 to days 0–7 after phase 7.

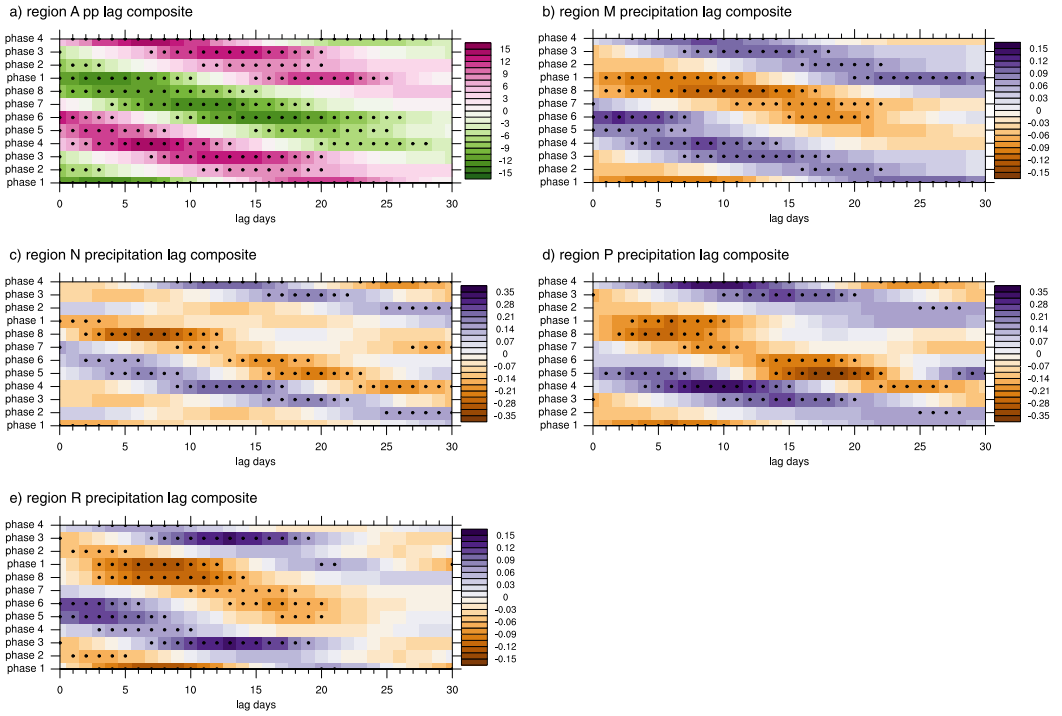

FIG. 7. (a) Lag composite of pp anomalies (hPa^2) in region A (shown in Fig. 6a). (b) Lag composite of precipitation anomalies (mm day^{-1}) in region M (52.0°–57.0°N, 97.5°–89°W; shown in Fig. 6c). (c)–(e) As in (b), but for regions N (42.5°–46.5°N, 97.0°–94.5°W), P (40.0°–43.5°N, 95°–88.5°W), and R (58.5°–61.0°N, 107.5°–103.5°W), respectively (regions shown in Fig. 6c). The dotted boxes in (a)–(e) are statistically significant at the 95% level from the results of a Monte Carlo test.

Comparing the storm-track anomaly over the eastern Pacific (Fig. 6e) and precipitation in California and Nevada (Fig. 6g), we find that the precipitation anomaly in California generally has the same sign with the storm-track anomaly in the eastern Pacific. Note that the storm-track anomaly signals generally lead the precipitation signals by several days. This is reasonable because precipitation in region I is on the downstream side of the storm-track region G. A similar precipitation anomaly can be found over New Mexico (region K; Fig. 6i).

The MJO-related precipitation anomaly is also important over British Columbia. The lag composite for region J (Fig. 6h) shows that the MJO-related precipitation anomaly in British Columbia has a nearly opposite signal to the precipitation signal in California (region I; Fig. 6g), especially during phases 2–4. This suggests that the MJO leads to a north–south shift of precipitation over the west coast of North America. Unlike California, where the precipitation variability can be highly explained by storm-track variability (Chang et al. 2015), the precipitation in British Columbia is not highly correlated with storm-track variability (not shown), which indicates that the precipitation variability in British Columbia cannot be solely explained by storm-track variability nearby. One of the possibilities is that the precipitation variability in British Columbia may be more related to variability of the onshore upslope zonal mean flow rather than storm-track variations (see discussions in section 6). Nevertheless, we can still see precipitation in British Columbia showing a similar pattern as the storm-track activity over western Canada (region H; Fig. 6f). Generally, when there is more precipitation in British Columbia, a positive storm-track activity anomaly can be found in western Canada. Also, the precipitation signal in British Columbia leads the storm-track signal in western Canada by a couple of days. Note that the storm-track signal in western Canada (Fig. 6f) also leads the signal in central Canada (region A; Fig. 5c), and they are very consistent. In summary, MJO can lead to shifts in precipitation as well as storm-track activity near the west coast of North America.

Next, we focus on storm-track activity in region A that has been discussed in section 4. Four regions, M, N, P, and R (Figs. 6c,d), have been selected where the precipitation anomaly has a high signal-to-noise ratio. The geographic location of these four regions indicates that they may be affected by storm-track activity in region A. The lag composites of precipitation to the southwest of Hudson Bay (region M; Fig. 7b), Minnesota (region N;

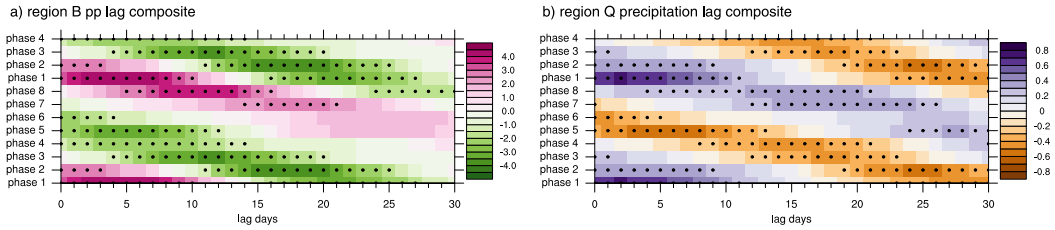

FIG. 8. (a) Lag composite of pp anomalies (hPa^2) in region B (shown in Fig. 6a). (b) Lag composite of precipitation anomalies ($mm\ day^{-1}$) in region Q (25.0°–32.0°N, 85°–80°W; shown in Fig. 6c). The dotted boxes in (a) and (b) are statistical significant at the 95% level from the results of a Monte Carlo test.

Fig. 7c), Iowa (region P; Fig. 7d), and to the west of the Hudson Bay (region R; Fig. 7e), are very similar to the storm-track activity lag composite of region B. This shows that MJO can have a significant impact on the precipitation over the central part of the continent, and it is very likely that the precipitation variability is induced by MJO-related storm-track variability. Note that the precipitation anomaly is statistically significant in region M and N even up to 45 days (not shown), but what gives rise to this extended period of significant precipitation anomalies is currently not clear. Our results of large MJO-related precipitation variability over region N are consistent with previous studies (Baxter et al. 2014; Becker et al. 2011; Zhou et al. 2012).

Finally, winter precipitation in Florida (region Q) is apparently related to the storm-track anomalies over region B. MJO can have a large impact on precipitation in Florida (Figs. 6c,d). The lag composite of storm-track activity in region B (Fig. 8a) and lag composite of precipitation in region Q (Fig. 8b) show very similar patterns. We can see that the precipitation in Florida is highly affected by the MJO and is highly correlated with the MJO-related storm-track variability over the southeastern United States.

6. MJO-related midlatitude variability and Rossby waves trains

What is the mechanism through which MJO can modify midlatitude circulation? Previous studies have shown that the MJO acts as a propagating heat source in the tropics. As discussed in section 1, previous studies have also shown that the midlatitude atmosphere will respond to tropical heating caused by propagation of Rossby wave trains excited by the heating anomaly. The Rossby waves modify the large-scale circulation, and can act to modulate storm-track activity, SAT, and precipitation. Many previous studies (e.g., Baxter et al. 2014; Guo et al. 2017) used an upper-level streamfunction to illustrate the Rossby wave response related to MJO. In addition to streamfunction anomalies, we also apply the WAF of Takaya and Nakamura (2001), which is a three-dimensional flux parallel to the group velocity of Rossby waves, to show the evolution of the stationary Rossby wave trains excited by the MJO. Here, we will mainly highlight composites from MJO phases that show streamfunction anomalies in the vicinity of North America that are consistent with the significant weather impacts discussed in the preceding sections.

The lag composites of streamfunction and WAF at 250 hPa, as well as the OLR anomalies, as a function of lag with respect to MJO phase 3, are shown in Fig. 9. Instead of showing the snapshots of streamfunction anomalies and WAF of each MJO phase at zero lag, the composites of different lags are shown, since the evolution of streamfunction anomalies and WAF (which will be discussed later) provide more insights on the MJO-forced midlatitude impact. Among all eight MJO phases, the lag composite of streamfunction anomalies and WAF in each phase is coherent with the lag composites of adjacent phases. The lag composites for phases 3 and 8 (composites for phases 1, 2, 4, 5, and 7 are shown in the supplemental material; phase 6 will be discussed later) show the clearest wave propagation to North America and the WAF in those two phases are the most distinctive. In addition, the temperature signal over the eastern United States (Fig. 5g) is largest after phases 3 and 8. Hence, we will first focus on these two phases. Note that the streamfunction anomalies and WAF composite are calculated in the time period of 1979–2016, while the OLR contours are composites of 1979–2013. Here we just use OLR contours to illustrate the enhanced and suppressed tropical convection. Although the lag composites have a 4-day interval for all MJO phases, we choose a different start date for phases 3 and 8 (day −12 for phase 3 and day −10 for phase 8) to better show when the important features of the Rossby wave develop.

In Fig. 9, color shadings define composite streamfunction anomalies and the red lines depict the 95%

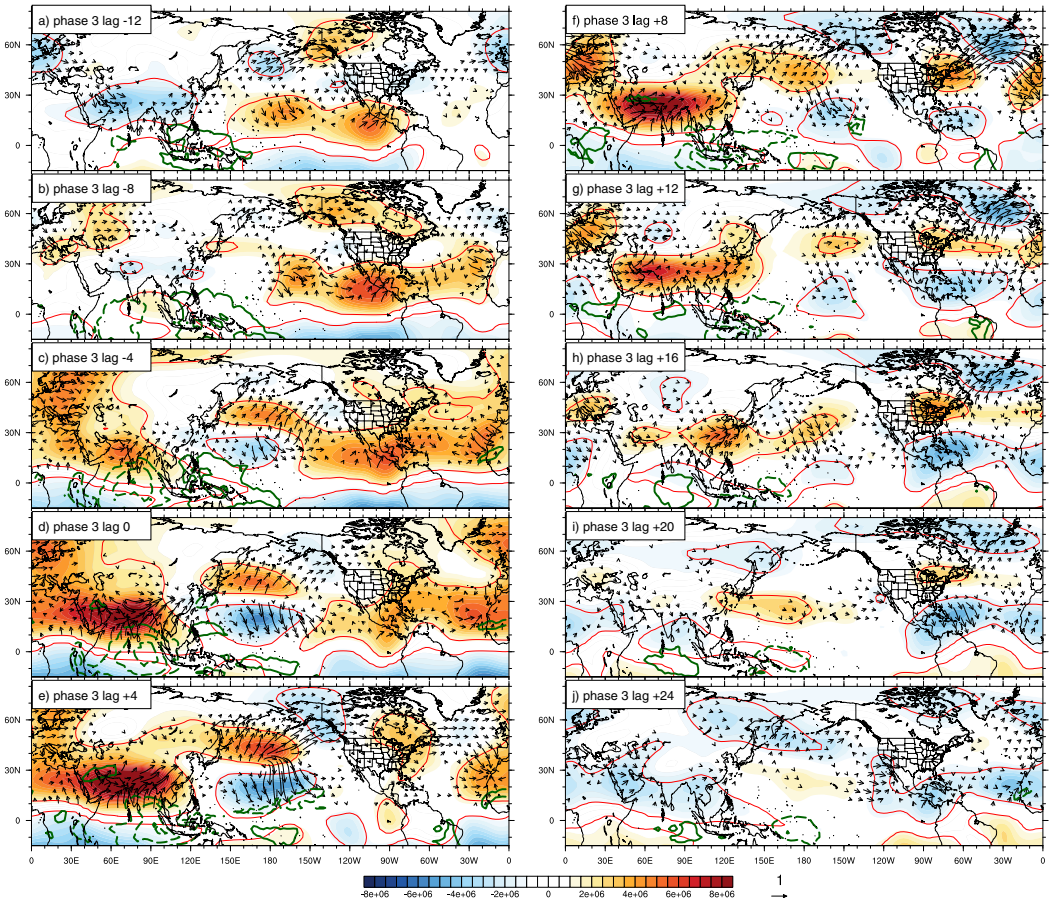

FIG. 9. The lag composite of streamfunction anomalies, WAF at 250 hPa, and OLR anomalies with respect to MJO phase 3. Composite of boreal winter OLR anomalies are in green contours. Solid contours are positive, dashed contours are negative, and the zero contour is omitted. Contour interval is 8 W m^{-2}. Color shading is the streamfunction anomaly ($m^2 s^{-1}$). The red contours outline the regions where the streamfunction anomaly is statistically significant at the 95% level from the results of a Monte Carlo test. Arrows are WAF associated with streamfunction anomalies. Only WAF greater than 0.1 $m^2 s^{-2}$ is plotted. The scaling for the arrows is shown at the bottom of the figure ($m^2 s^{-2}$).

statistical significance level from a Monte Carlo test. Most of the anomaly signals in Fig. 9 are statistically significant. Green contours in the figure show the OLR anomalies that generally resemble the tropical convection anomalies associated with the MJO. The arrows show the WAF. Since the WAF is derived under quasigeostrophic assumptions, only the WAF north of 5°N is shown in the composites.

From 8 to 4 days prior to MJO phase 3, convection in the Indian Ocean is enhanced, and convection in the Maritime Continent is suppressed (Figs. 9b and 9c, respectively). This convection pattern resembles MJO phases 1 and 2 (e.g., Wheeler and Hendon 2004). On day −4 (Fig. 9c), enhanced tropical convection over the Indian Ocean leads to upper-level vortex compression, which results in anomalous anticyclonic flow north of the enhanced convection center; similarly, an upper-level cyclonic anomaly is found over the western Pacific related to the suppressed convection over the Maritime Continent. A Rossby wave train starts from this cyclonic anomaly, with an anticyclonic anomaly already emerging north of the cyclonic anomaly on day −4. The WAF is generally northward over the Pacific just to the east of Asia, and the WAF identifies the propagation of the wave train as it moves into the midlatitudes. Around lag day 0 (Fig. 9d), when the MJO is in phase 3, the convection center moves eastward to the eastern part of the Indian Ocean and the western part of the Maritime Continent and becomes stronger. The accompanying upper-level anticyclonic anomaly is also enhanced. The WAF shows that the Rossby wave train related to the enhanced convection propagates to the northeast. Seo et al. (2016) suggested that the southward WAF over the eastern part of the cyclonic anomaly is generally because

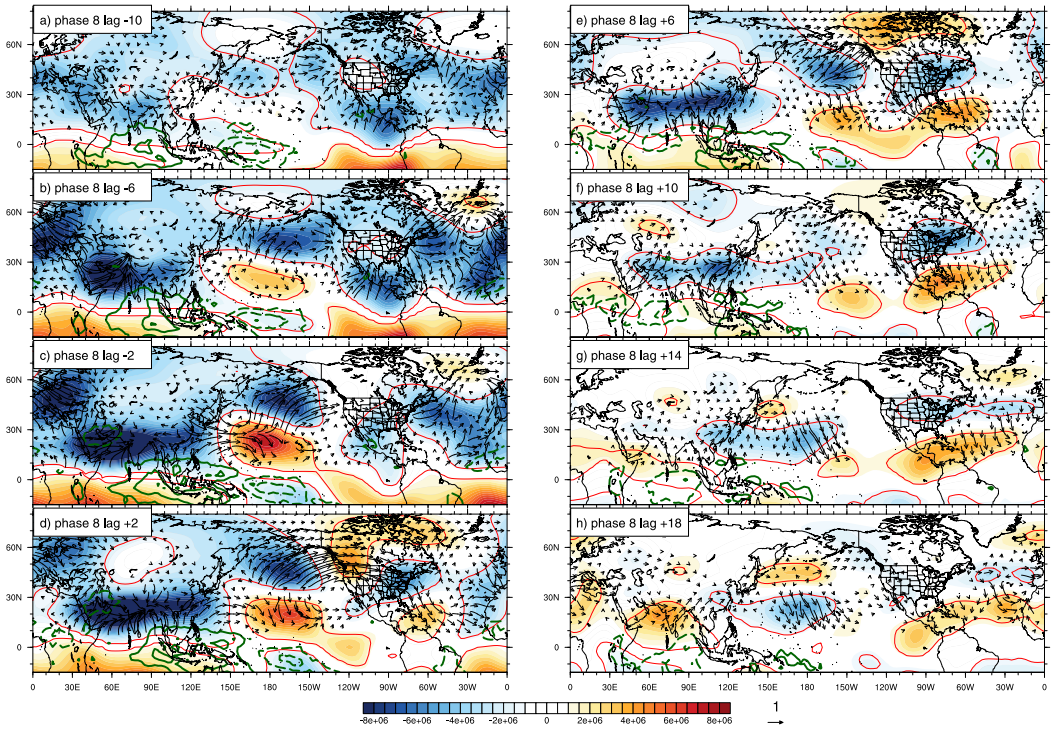

FIG. 10. As in Fig. 9, but with respect to MJO phase 8.

of the reflection of larger wavenumber Rossby waves that then propagate to the south. The WAF from the anticyclonic anomaly in the midlatitude western Pacific points northeastward, and a cyclonic anomaly starts to develop over the Gulf of Alaska. On day +4 (Fig. 9e), a very clear wave train has developed, and an anticyclonic anomaly starts to develop over northeastern North America. The WAF clearly indicates that this anticyclonic anomaly has developed from the cyclonic anomaly over Alaska and the Gulf of Alaska. The wave train originated from the subtropical western Pacific prior to day −4, has propagated all the way to northeastern North America by day +4, with the wave trajectory generally following a great circle. Around day +8 (Fig. 9f), a well-developed anticyclonic anomaly covers the northeastern United States and southeastern Canada. Clearly, this anomaly is related to the warm anomaly over the eastern United States, as well as the north–south storm-track shift over North America after phase 3 (Fig. 5). The wave train continues to propagate across the Atlantic into Europe during days from +8 to +16. This result is very consistent with those of Lin et al. (2009), which showed very similar WAF at 200 hPa over the Atlantic in the two-pentad lag composite of MJO phase 3. The anticyclonic anomaly over the northern United States gradually weakens after day +8.

Figure 10 shows the lag composites of streamfunction anomalies and WAF related to MJO phase 8. At day −10 (Fig. 10a), tropical convection is suppressed over the Indian Ocean and enhanced to the east of the Maritime Continent. Around day −6 (Fig. 10b), a cyclonic anomaly strengthens to the northwest of the suppressed convection, and an anticyclonic anomaly strengthens to the north of the enhanced convection over the subtropical central Pacific. This anticyclonic anomaly acts as a vorticity source, and Rossby wave propagation toward the midlatitudes is indicated by the WAF, leading to the strengthening of a cyclonic anomaly over the midlatitude Pacific. This creates a dipole structure of streamfunction anomalies, and the subtropical jet over the Pacific is strengthened. The dipole structure strengthened on day −2 (Fig. 10c), as the anticyclonic anomaly is strengthened not only by the enhanced convection, but also by WAF from the west originating from the cyclonic anomaly over South Asia. Around day +2 (Fig. 10d), the Rossby wave can be seen to propagate across North America. A very clear wave train emerges with an anticyclonic anomaly over western Canada, a cyclonic anomaly over the eastern United States, and an anticyclonic anomaly over the Caribbean Sea. The WAF clearly shows the direction of the wave propagation, and the amplitude of WAF is relatively strong at this time. For the lag composites after day +6

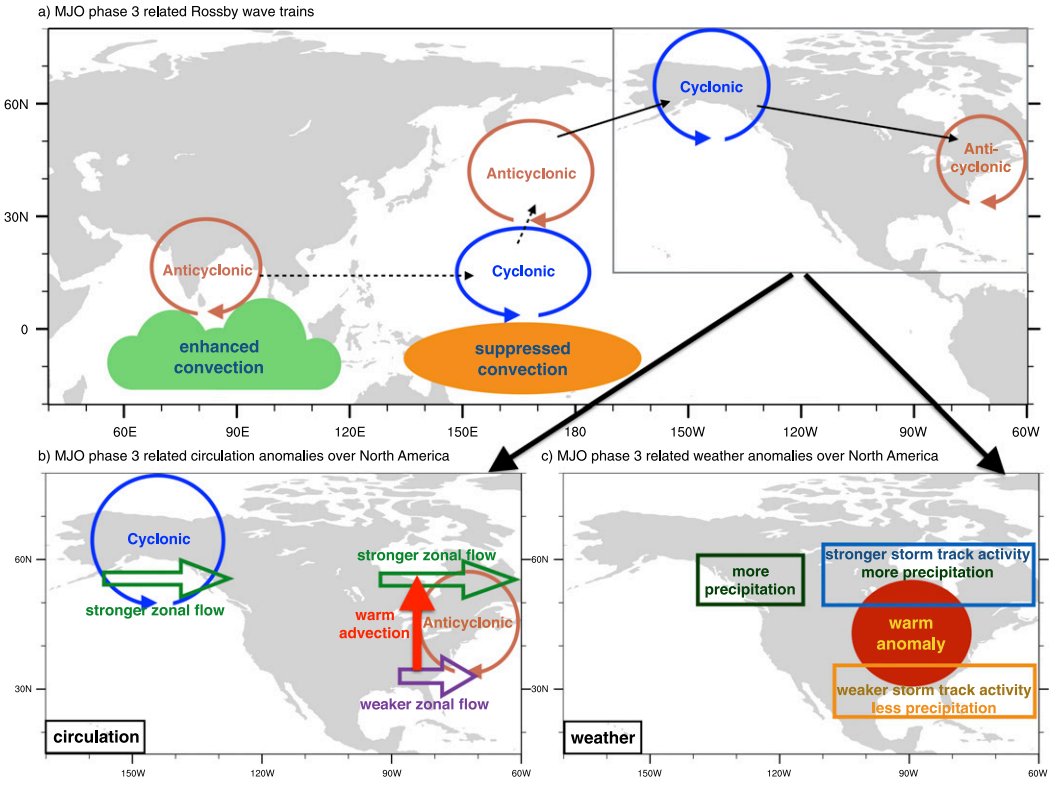

FIG. 11. Schematic diagrams showing MJO phase 3 related Rossby wave train and its impact over North America. (a) MJO phase 3 related tropical convection anomalies and Rossby wave train. Also shown are the Rossby wave train's impact over North America on (b) circulation and (c) weather. A similar schematic can be applied to phase 8 by reversing the sign of the circulation and related weather anomalies and shifting the pattern slightly eastward.

(Figs. 10e–h), we can see the wave train gradually dissipates.

Figure 11a shows a schematic diagram summarizing the Rossby wave train related to MJO phases 3 and 8. The sign of the anomalies correspond to that of phase 3, and the schematic for phase 8 mainly has anomalies with opposite signs[1] that are displaced slightly eastward. The arrows between the circulation anomalies over the subtropics and western Pacific are dashed since the WAF connection between these anomalies are not very clear for phase 3 but are much clearer for phase 8.

How do those upper-level stationary Rossby waves play a role on the surface weather? The schematic shown in Figs. 11b and 11c describes their connection. From lag days +4 to +20 after phase 3, an anticyclonic anomaly persists over the northeastern United States and southeastern Canada (Fig. 9). Together with the cyclonic anomalies north and south of it, this anticyclonic anomaly strengthens the zonal flow to the north over Canada (Fig. 11b), a region corresponding to region A in Fig. 5a. These anomalies also weaken the zonal flow in the south (over the southeastern United States, similar region as region B in Fig. 5a). As stronger mean flow generally results in enhanced storminess, thus the storm track in region A is enhanced (Fig. 11c) during the same time in the lag composite (Fig. 5e). Because of weaker mean flow, storm-track activity in region B is suppressed (Figs. 11c and 5f). Seo et al. (2016) has shown that the MJO influences the midlatitude temperature mainly by horizontal temperature advection. The western part of the anticyclonic anomaly, which is equivalent barotropic and extends to the lower levels (not shown), brings warm advection (Fig. 11b) and induces the warm anomaly (Fig. 11c) over the eastern United States (region C in Figs. 5c,g). The cyclonic anomaly over Alaska, which exists from lag days +4 to +12 after phase 3 (Fig. 9), strengthens the zonal flow over the west coast of Canada, and brings more precipitation to the coastal regions (Figs. 11b,c; see also region J in Figs. 6c,h). During lag days from +2 to +14 in phase 8 (Fig. 10), we generally see an opposite signal to phase 3. A cyclonic anomaly is over

[1] The only difference is that Rossby wave propagation is in the same direction since WAF is quadratic and the direction is independent of the sign of the streamfunction anomaly.

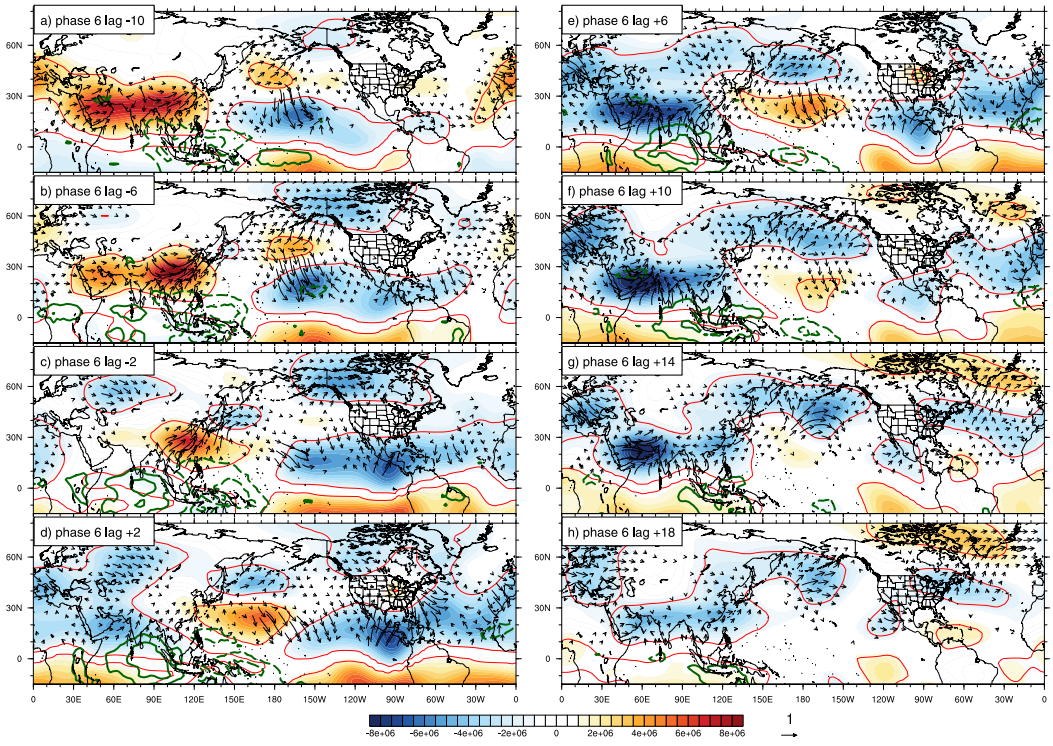

FIG. 12. As in Fig. 9, but with respect to MJO phase 6.

the eastern part of North America. The streamfunction anomalies indicate that the zonal flow is weaker to the north and stronger to the south, which is consistent with weaker storm-track activity to the north (region A; Fig. 5e) and stronger storm-track activity to the south (region B; Fig. 5f). Also, cold advection west of the cyclonic anomaly gives rise to the cold anomaly over the eastern United States. The anticyclonic anomaly over Alaska weakens the zonal mean flow over the west coast of Canada and results in less precipitation (region J; Fig. 6h). Patterns with opposite sign of the anomalies in Figs. 11b and 11c can describe how the Rossby wave related to MJO phase 8 influences the circulation and weather over North America. The lifetime of the streamfunction anomaly over the eastern part of the continent is longer after phase 3 (anticyclonic; Fig. 9) and shorter after phase 8 (cyclonic; Fig. 10), this explains why there are more days with weaker storm-track activity in region B (Fig. 5d) and more days with a warm anomaly in region C (Fig. 5g).

As shown in Seo et al. (2016), the MJO-generated Rossby waves are characterized by stationary zonal wavenumbers 2–4. Henderson et al. (2017) showed that the MJO Rossby wave trains should propagate along the stationary wavenumber contours. The stationary wavenumber can be derived from the distribution of the mean flow. From Fig. 3 of Henderson et al. (2017), one can see that the pathway for the MJO-induced Rossby wave trains should be starting in subtropical western Pacific, going eastward to central Pacific, northeastward to Alaska, then southeastward to the eastern part of North America, and finally northeastward across the Atlantic (following wavenumber-3 contours). Therefore, MJO phases that can produce vorticity anomalies in the western Pacific may initiate Rossby wave trains that modify the weather over North America. In both phase 3 and 8 WAF composites, the enhanced (suppressed) tropical convection provides strong vorticity anomalies over the western Pacific, thus acting as Rossby wave sources to excite wave trains that propagate toward North America.

Figure 12 shows the lag composite of the streamfunction anomaly and WAF related to MJO phase 6. Around lag day −10 (Fig. 12a), the anomalous convection center is over the Maritime Continent. A strong anticyclonic anomaly is to the northwest of the positive convection anomaly. During lag days from −6 to +2 (Figs. 12b–d), as the MJO propagates eastward and the convection is suppressed over the Indian Ocean, the anticyclonic anomaly also moves eastward. A cyclonic anomaly develops north of the anticyclonic anomaly during the same time, because of the propagation of

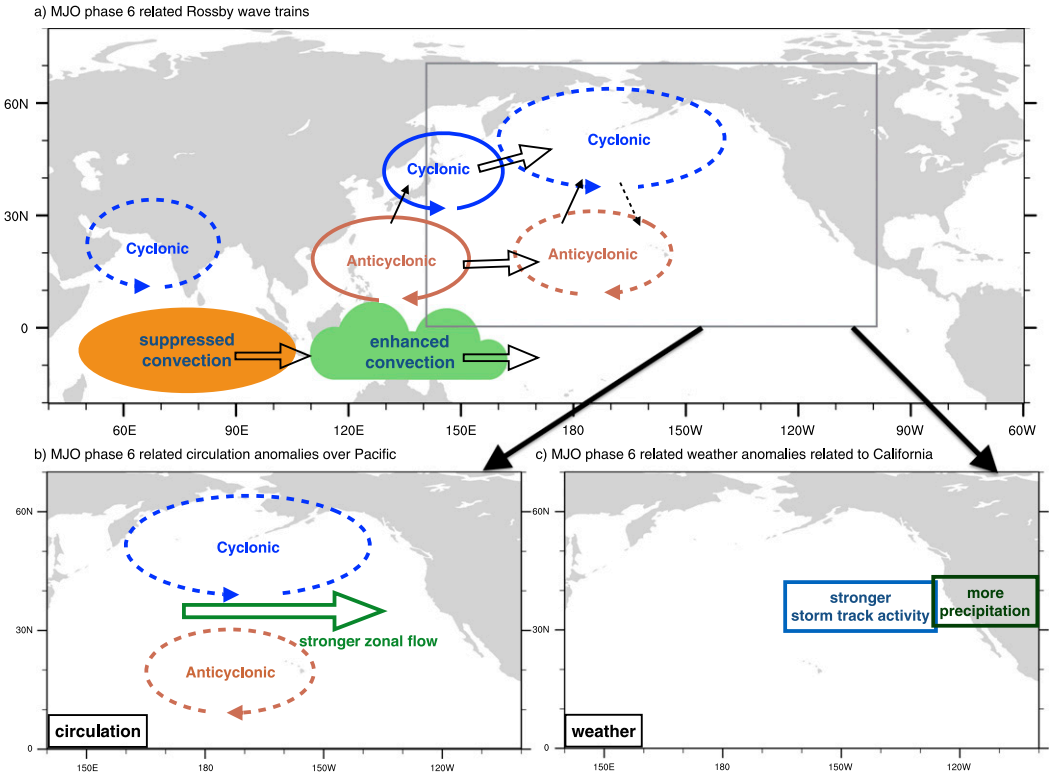

FIG. 13. As in Fig. 11, but for MJO phase 6 and its impacts over the Pacific and California. In (a) the solid (dashed) cyclonic and anticyclonic anomalies represent the circulation anomalies around lag day 0 (+6). Hollow arrows represent the eastward propagation of the convection anomalies and circulation anomalies. A similar schematic can be applied to phase 2 by reversing the sign of the circulation and related weather anomalies.

Rossby wave as indicated by the WAF. During lag days from +2 to +6 (Figs. 12d,e), shorter Rossby waves get reflected at the east part of the cyclonic and anticyclonic anomalies, and the anomalies extend eastward toward the eastern Pacific. This Rossby wave propagation process described above is also shown in a schematic diagram(Fig. 13a). In between the cyclonic and anticyclonic anomalies during lag days from +6 to +10 (Figs. 12e,f), the zonal flow is enhanced (Fig. 13b). As the zonal jet extension reaches the eastern Pacific, the storm-track activity over the eastern Pacific gets stronger (phase 6 in region G; Figs. 6e and 13c). We also see more precipitation over California several days later (Figs. 6g and 13c), which is consistent with the results of Chang et al. (2015) that stronger storm-track activity over the eastern Pacific results in more precipitation over California. Correspondingly, the lag composites for phase 2 (Fig. S2 in the supplemental material) during lag days from +6 to +10 shows the opposite circulation anomalies and the jet weakens over the eastern Pacific, which is consistent with the reduction of storm-track activity (Fig. 6e) and precipitation (Fig. 6g) after lag day +10 in phase 2.

Figure 6g also shows positive precipitation anomalies over California at short lags after phases 1 and 2. These are apparently related to an anticyclonic anomaly over the tropical eastern Pacific extending into Mexico, bringing enhanced westerlies to California (Fig. S1e in the supplemental material). This anticyclone seems to have formed over the tropical central Pacific in response to enhanced convection to its south and gradually moved and extended eastward.

While these lag composites are indicative of the MJO being important in exciting wave trains to impact North America, it is not clear how the interplay between the eastward propagation of the MJO and the Rossby waves generated by the heating might impact the propagation of the waves toward North America. Detailed modeling studies will be needed to answer this question.

7. Summary

Many previous studies have shown that MJO can have significant impacts on wintertime temperature, precipitation, and storm-track activity on intraseasonal

time scales. Note, however, that factors other than MJO (e.g., PNA pattern), can also play an important role in weather over North America on intraseasonal time scales. In this study, a new lag composite strategy has been developed to comprehensively show the impact of the MJO during the entire MJO life cycle and at different lags. This lag composite strategy provides information about which regions MJO plays an important role in surface weather on weekly to monthly time scales. The results show that MJO has significant impacts on surface weather over North America. For storm-track activity, the most significant impacts are found in central Canada, the southeastern United States, and the eastern Pacific. Consistent with previous studies, MJO has a strong influence on the temperature near the Arctic, with the eastern United States seemingly the only region in the midlatitudes where the MJO-related temperature anomaly is large both in amplitude and signal-to-noise ratio. The regions where MJO has large impacts on precipitation are rather scattered, but significant signals can be found over the western, central, and southeastern United States.

The lag composites show that MJO leads to a north–south shift of storm-track activity over Canada and the southeastern United States. Surface air temperate is also highly influenced by the MJO over the eastern United States and Alaska. The north–south shift of storm-track activity is consistent with the change in temperature gradient related to the MJO. In addition, MJO gives rise to the strengthening and weakening of storm-track activity over the eastern Pacific, leading to enhanced or reduced precipitation over the U.S. Southwest. An MJO-related north–south shift of precipitation is also found over the west coast of North America. As MJO can modify the atmospheric river events in the eastern Pacific (e.g., Mundhenk et al. 2016; Guan and Waliser 2015), this result is within our expectation. Over the west coast of North America, the Ohio River valley, and Florida, MJO modification of precipitation is significant, and the precipitation signal is consistent with the MJO-related storm-track activity signal nearby, which indicates that MJO modifies the precipitation through modifying the storm-track activity.

Rossby wave trains excited by the MJO are often considered to show how the MJO influences surface weather in the extratropics. Those wave trains are clearly found in lag composites based on the MJO phases. For example (Fig. 11), the tropical enhanced and suppressed convection around phase 3 (phase 8) excite the anticyclonic (cyclonic) anomaly over South Asia and cyclonic (anticyclonic) anomalies over the western Pacific. These circulation anomalies provide the sources for the Rossby wave trains, and these wave trains propagate across the Pacific and North America, bringing upper-level anticyclonic and cyclonic flow anomalies over the eastern part of North America, respectively. The anticyclonic (cyclonic) anomaly gives rise to the northward (southward) shift of the storm track as it strengthens the zonal flow to the north (south), and the associated warm (cold) advection west of the anticyclonic (cyclonic) anomaly brings warmer (colder) temperatures to the eastern United States. The cyclonic (anticyclonic) anomaly over Alaska also strengthens (weakens) the zonal flow over the west coast of Canada and brings more (less) precipitation. The Rossby wave train related to MJO phase 6 (phase 2) can also induce stronger (weaker) storm-track activity over California by enhancing (reducing) the jet stream over the eastern Pacific, which results in more (less) precipitation over California (Fig. 13). Currently, we are unable to separate the midlatitude impact of adjacent MJO phases (e.g., the difference of impact between phases 2 and 3). Our hypothesis is that because of the quasi-periodicity of the MJO phases, remote anomalies forced by one MJO phase may appear to be also connected with the other phases. In the schematic diagrams (Figs. 11 and 13), we mainly focus on the impacts over North America related to the Rossby wave trains that we can clearly trace backward to the MJO convection anomalies based on lagged correlations from a single phase. Thus, Figs. 11 and 13 might not include all possible MJO-related impacts.

In this study, we have used composite analyses to show the impact of MJO on surface weather over North America. The detailed dynamics involved still need to be examined using modeling studies. In addition, given that the MJO phase can be predicted out to three to four weeks in advance (e.g., Kim et al. 2014), it is expected that the MJO-forced signals over the midlatitudes should be predictable through the subseasonal time scale. We are currently assessing how successful our climate models are in predicting these signals.

Acknowledgments. This research has been conducted as part of the NOAA MAPP S2S Prediction Task Force and supported by NOAA Grant NA16OAR4310070. Kim was also supported by the KMA Research and Development Program under Grant KMI2018-03110. Zhang was also supported by the U.S. National Science Foundation. The authors would also like to thank two anonymous reviewers for comments that have helped to clarify and improve this paper.

APPENDIX

The Monte Carlo Procedure

For each grid point, the Monte Carlo procedure generates 10 000 random composites that are similar to Fig. 1b. Each random composite is produced as follows. 1) Continuous days when the RMM index amplitude is greater than 1 are defined as an MJO event. We count the number of events x and number of days in each event $N(x)$ during 1979–2016 boreal winter. For day number j in event number i, the MJO phase is denoted as phase(i, j). 2) A total number of x random dates in the boreal winter are generated. These dates will be considered as the starting dates of all the ''MJO'' events in this random composite. 3) For event number i' in the random composite, the days from the starting date to $[N(i') - 1]$ days after the starting date are considered in this ''MJO event.'' The number j' day in this event is considered in MJO phase(i', j'). 4) As we have the information about when the MJO events happen and which phase each day is in, we can produce the random composite. Note that with the procedure described above, each random composite will have the same number of MJO events as the actual MJO composite (e.g., Fig. 1b), and the number of days in each event is the same as that in the actual MJO composite as well. Therefore, the total number of days in each MJO phase in the random composite is the same as that in the actual composite. As these features of MJO are preserved in the Monte Carlo procedure, the statistical significance level can be obtained from the random composites. To assess the statistical significance level, for example, in Fig. 1b, $\mathrm{pp}'_{\mathrm{MJO}}(\mathrm{phase}_{\mathrm{MJO}}, \mathrm{day}_{\mathrm{lag}})$ in the 10 000 random composites is ranked in an ascending order for each phase and each lag day. If $\mathrm{pp}'_{\mathrm{MJO}}(\mathrm{phase}_{\mathrm{MJO}}, \mathrm{day}_{\mathrm{lag}})$ in the actual composite is smaller than the rank number 500 (bottom 5% of 10 000) or greater than the rank number 9500 (top 5% of 10 000) composite in that phase and lag day, then $\mathrm{pp}'_{\mathrm{MJO}}(\mathrm{phase}_{\mathrm{MJO}}, \mathrm{day}_{\mathrm{lag}})$ is considered to be statistically significant at 95%. The significance level of the MJO-related anomalies over all eight phases and lag days 0–30 in (e.g., Fig. 2c) is derived by applying the method described above but using $\mathrm{pp}'^{2}_{\mathrm{MJO}}$ at each grid point.

REFERENCES

Baxter, S., S. Weaver, J. Gottschalck, and Y. Xue, 2014: Pentad evolution of wintertime impacts of the Madden–Julian oscillation over the contiguous United States. *J. Climate*, **27**, 7356–7367, https://doi.org/10.1175/JCLI-D-14-00105.1.

Becker, E. J., E. H. Berbery, and R. W. Higgins, 2011: Modulation of cold-season U.S. daily precipitation by the Madden–Julian oscillation. *J. Climate*, **24**, 5157–5166, https://doi.org/10.1175/2011JCLI4018.1.

Blackmon, M. L., 1976: A climatological spectral study of the 500 mb geopotential height of the Northern Hemisphere. *J. Atmos. Sci.*, **33**, 1607–1623, https://doi.org/10.1175/1520-0469(1976)033<1607:ACSSOT>2.0.CO;2.

Bond, N. A., and G. A. Vecchi, 2003: The influence of the Madden–Julian oscillation on precipitation in Oregon and Washington. *Wea. Forecasting*, **18**, 600–613, https://doi.org/10.1175/1520-0434(2003)018<0600:TIOTMO>2.0.CO;2.

Cassou, C., 2008: Intraseasonal interaction between the Madden–Julian oscillation and the North Atlantic Oscillation. *Nature*, **455**, 523–527, https://doi.org/10.1038/nature07286.

Chang, E. K. M., S. Lee, and K. L. Swanson, 2002: Storm track dynamics. *J. Climate*, **15**, 2163–2183, https://doi.org/10.1175/1520-0442(2002)015<02163:STD>2.0.CO;2.

——, C. Zheng, P. Lanigan, A. M. W. Yau, and J. D. Neelin, 2015: Significant modulation of variability and projected change in California winter precipitation by extratropical cyclone activity. *Geophys. Res. Lett.*, **42**, 5983–5991, https://doi.org/10.1002/2015GL064424.

Chen, M., and Coauthors, 2008: CPC unified gauge-based analysis of global daily precipitation. Western Pacific Geophysics Meeting, Cairns, Australia, Amer. Geophys. Union, 14 pp., http://ftp.cpc.ncep.noaa.gov/precip/CPC_UNI_PRCP/GAUGE_GLB/DOCU/Chen_et_al_2008_Daily_Gauge_Anal.pdf.

Dee, D. P., and Coauthors, 2011: The ERA-Interim reanalysis: Configuration and performance of the data assimilation system. *Quart. J. Roy. Meteor. Soc.*, **137**, 553–597, https://doi.org/10.1002/qj.828.

Deng, Y., and T. Jiang, 2011: Intraseasonal modulation of the North Pacific storm track by tropical convection in boreal winter. *J. Climate*, **24**, 1122–1137, https://doi.org/10.1175/2010JCLI3676.1.

Donald, A., H. Meinke, B. Power, A. de H. N. Maia, M. C. Wheeler, N. White, R. C. Stone, and J. Ribbe, 2006: Near-global impact of the Madden-Julian Oscillation on rainfall. *Geophys. Res. Lett.*, **33**, L09704, https://doi.org/10.1029/2005GL025155.

Flatau, M., and Y. Kim, 2013: Interaction between the MJO and polar circulations. *J. Climate*, **26**, 3562–3574, https://doi.org/10.1175/JCLI-D-11-00508.1.

Grise, K. M., S. Son, and J. R. Gyakum, 2013: Intraseasonal and interannual variability in North American storm tracks and its relationship to equatorial Pacific variability. *Mon. Wea. Rev.*, **141**, 3610–3625, https://doi.org/10.1175/MWR-D-12-00322.1.

Guan, B., and D. E. Waliser, 2015: Detection of atmospheric rivers: Evaluation and application of an algorithm for global studies. *J. Geophys. Res. Atmos.*, **120**, 12 514–12 535, https://doi.org/10.1002/2015JD024257.

——, ——, N. P. Molotch, E. J. Fetzer, and P. J. Neiman, 2012: Does the Madden–Julian oscillation influence wintertime atmospheric rivers and snowpack in the Sierra Nevada? *Mon. Wea. Rev.*, **140**, 325–342, https://doi.org/10.1175/MWR-D-11-00087.1.

Guo, Y., T. Shinoda, J. Lin, and E. K. Chang, 2017: Variations of Northern Hemisphere storm track and extratropical cyclone activity associated with the Madden–Julian oscillation. *J. Climate*, **30**, 4799–4818, https://doi.org/10.1175/JCLI-D-16-0513.1.

Harvey, B. J., L. C. Shaffrey, and T. J. Woollings, 2014: Equator-to-pole temperature differences and the extra-tropical storm

track responses of the CMIP5 climate models. *Climate Dyn.*, **43**, 1171, https://doi.org/10.1007/s00382-013-1883-9.

Henderson, S. A., E. D. Maloney, and S. Son, 2017: Madden–Julian oscillation Pacific teleconnections: The impact of the basic state and MJO representation in general circulation models. *J. Climate*, **30**, 4567–4587, https://doi.org/10.1175/JCLI-D-16-0789.1.

Higgins, R. W., J. E. Schemm, W. Shi, and A. Leetmaa, 2000: Extreme precipitation events in the western United States related to tropical forcing. *J. Climate*, **13**, 793–820, https://doi.org/10.1175/1520-0442(2000)013<0793:EPEITW>2.0.CO;2.

Hoskins, B. J., and D. J. Karoly, 1981: The steady linear response of a spherical atmosphere to thermal and orographic forcing. *J. Atmos. Sci.*, **38**, 1179–1196, https://doi.org/10.1175/1520-0469(1981)038<1179:TSLROA>2.0.CO;2.

Jin, F., and B. J. Hoskins, 1995: The direct response to tropical heating in a baroclinic atmosphere. *J. Atmos. Sci.*, **52**, 307–319, https://doi.org/10.1175/1520-0469(1995)052<0307:TDRTTH>2.0.CO;2.

Jones, C., 2000: Occurrence of extreme precipitation events in California and relationships with the Madden–Julian oscillation. *J. Climate*, **13**, 3576–3587, https://doi.org/10.1175/1520-0442(2000)013<3576:OOEPEI>2.0.CO;2.

——, and L. M. Carvalho, 2012: Spatial–intensity variations in extreme precipitation in the contiguous United States and the Madden–Julian oscillation. *J. Climate*, **25**, 4898–4913, https://doi.org/10.1175/JCLI-D-11-00278.1.

Kiladis, G. N., J. Dias, K. H. Straub, M. C. Wheeler, S. N. Tulich, K. Kikuchi, K. M. Weickmann, and M. J. Ventrice, 2014: A comparison of OLR and circulation-based indices for tracking the MJO. *Mon. Wea. Rev.*, **142**, 1697–1715, https://doi.org/10.1175/MWR-D-13-00301.1.

Kim, H. M., P. J. Webster, V. E. Toma, and D. Kim, 2014: Predictability and prediction skill of the MJO in two operational forecasting systems. *J. Climate*, **27**, 5364–5378, https://doi.org/10.1175/JCLI-D-13-00480.1.

Kunkel, K. E., D. R. Easterling, D. A. Kristovich, B. Gleason, L. Stoecker, and R. Smith, 2012: Meteorological causes of the secular variations in observed extreme precipitation events for the conterminous United States. *J. Hydrometeor.*, **13**, 1131–1141, https://doi.org/10.1175/JHM-D-11-0108.1.

Lau, N., 1978: On the three-dimensional structure of the observed transient eddy statistics of the Northern Hemisphere wintertime circulation. *J. Atmos. Sci.*, **35**, 1900–1923, https://doi.org/10.1175/1520-0469(1978)035<1900:OTTDSO>2.0.CO;2.

Lee, Y.-Y., and G.-H. Lim, 2012: Dependency of the North Pacific winter storm tracks on the zonal distribution of MJO convection. *J. Geophys. Res.*, **117**, D14101, https://doi.org/10.1029/2011JA017246.

L'Heureux, M. L., and R. W. Higgins, 2008: Boreal winter links between the Madden–Julian oscillation and the Arctic Oscillation. *J. Climate*, **21**, 3040–3050, https://doi.org/10.1175/2007JCLI1955.1.

Liebmann, B., and C. A. Smith, 1996: Description of a complete (interpolated) outgoing longwave radiation dataset. *Bull. Amer. Meteor. Soc.*, **77**, 1275–1277, https://doi.org/10.1175/1520-0477-77.6.1274.

Lin, H., and G. Brunet, 2009: The influence of the Madden–Julian oscillation on Canadian wintertime surface air temperature. *Mon. Wea. Rev.*, **137**, 2250–2262, https://doi.org/10.1175/2009MWR2831.1.

——, ——, and J. Derome, 2009: An observed connection between the North Atlantic Oscillation and the Madden–Julian oscillation. *J. Climate*, **22**, 364–380, https://doi.org/10.1175/2008JCLI2515.1.

——, ——, and R. Mo, 2010: Impact of the Madden–Julian oscillation on wintertime precipitation in Canada. *Mon. Wea. Rev.*, **138**, 3822–3839, https://doi.org/10.1175/2010MWR3363.1.

Ma, C., and E. K. Chang, 2017: Impacts of storm-track variations on wintertime extreme weather events over the continental United States. *J. Climate*, **30**, 4601–4624, https://doi.org/10.1175/JCLI-D-16-0560.1.

Madden, R. A., and P. R. Julian, 1971: Detection of a 40–50 day oscillation in the zonal wind in the tropical Pacific. *J. Atmos. Sci.*, **28**, 702–708, https://doi.org/10.1175/1520-0469(1971)028<0702:DOADOI>2.0.CO;2.

——, and ——, 1972: Description of global-scale circulation cells in the tropics with a 40–50 day period. *J. Atmos. Sci.*, **29**, 1109–1123, https://doi.org/10.1175/1520-0469(1972)029<1109:DOGSCC>2.0.CO;2.

——, and ——, 1994: Observations of the 40–50-day tropical oscillation—A review. *Mon. Wea. Rev.*, **122**, 814–837, https://doi.org/10.1175/1520-0493(1994)122<0814:OOTDTO>2.0.CO;2.

Matsueda, S., and Y. Takaya, 2015: The global influence of the Madden–Julian oscillation on extreme temperature events. *J. Climate*, **28**, 4141–4151, https://doi.org/10.1175/JCLI-D-14-00625.1.

Matthews, A. J., B. J. Hoskins, and M. Masutani, 2004: The global response to tropical heating in the Madden–Julian oscillation during the northern winter. *Quart. J. Roy. Meteor. Soc.*, **130**, 1991–2011, https://doi.org/10.1256/qj.02.123.

Mo, K. C., and R. W. Higgins, 1998: Tropical convection and precipitation regimes in the western United States. *J. Climate*, **11**, 2404–2423, https://doi.org/10.1175/1520-0442(1998)011<2404:TCAPRI>2.0.CO;2.

Mori, M., and M. Watanabe, 2008: The growth and triggering mechanisms of the PNA: A MJO-PNA coherence. *J. Meteor. Soc. Japan*, **86**, 213–236, https://doi.org/10.2151/jmsj.86.213.

Mundhenk, B., E. A. Barnes, and E. Maloney, 2016: All-season climatology and variability of atmospheric river frequencies over the North Pacific. *J. Climate*, **29**, 4885–4903, https://doi.org/10.1175/JCLI-D-15-0655.1.

Riddle, E. E., M. B. Stoner, N. C. Johnson, M. L. L'Heureux, D. C. Collins, and S. B. Feldstein, 2013: The impact of the MJO on clusters of wintertime circulation anomalies over the North American region. *Climate Dyn.*, **40**, 1749–1766, https://doi.org/10.1007/s00382-012-1493-y.

Sardeshmukh, P. D., and B. J. Hoskins, 1988: The generation of global rotational flow by steady idealized tropical divergence. *J. Atmos. Sci.*, **45**, 1228–1251, https://doi.org/10.1175/1520-0469(1988)045<1228:TGOGRF>2.0.CO;2.

Schreck, C. J., J. M. Cordeira, and D. Margolin, 2013: Which MJO events affect North American temperatures? *Mon. Wea. Rev.*, **141**, 3840–3850, https://doi.org/10.1175/MWR-D-13-00118.1.

Seo, K., and S. Son, 2012: The global atmospheric circulation response to tropical diabatic heating associated with the Madden–Julian oscillation during northern winter. *J. Atmos. Sci.*, **69**, 79–96, https://doi.org/10.1175/2011JAS3686.1.

——, H. Lee, and D. M. Frierson, 2016: Unraveling the teleconnection mechanisms that induce wintertime temperature anomalies over the Northern Hemisphere continents in response to the MJO. *J. Atmos. Sci.*, **73**, 3557–3571, https://doi.org/10.1175/JAS-D-16-0036.1.

Takaya, K., and H. Nakamura, 2001: A formulation of a phase-independent wave-activity flux for stationary and migratory

quasigeostrophic eddies on a zonally varying basic flow. *J. Atmos. Sci.*, **58**, 608–627, https://doi.org/10.1175/1520-0469(2001)058<0608:AFOAPI>2.0.CO;2.

Vecchi, G. A., and N. A. Bond, 2004: The Madden-Julian Oscillation (MJO) and northern high latitude wintertime surface air temperatures. *Geophys. Res. Lett.*, **31**, L04104, https://doi.org/10.1029/2003GL018645.

Wallace, J. M., G. Lim, and M. L. Blackmon, 1988: Relationship between cyclone tracks, anticyclone tracks and baroclinic waveguides. *J. Atmos. Sci.*, **45**, 439–462, https://doi.org/10.1175/1520-0469(1988)045<0439:RBCTAT>2.0.CO;2.

Wheeler, M. C., and H. H. Hendon, 2004: An all-season real-time multivariate MJO index: Development of an index for monitoring and prediction. *Mon. Wea. Rev.*, **132**, 1917–1932, https://doi.org/10.1175/1520-0493(2004)132<1917:AARMMI>2.0.CO;2.

Yoo, C., S. Feldstein, and S. Lee, 2011: The impact of the Madden-Julian Oscillation trend on the Arctic amplification of surface air temperature during the 1979–2008 boreal winter. *Geophys. Res. Lett.*, **38**, L24804, https://doi.org/10.1029/2011GL049881.

——, S. Lee, and S. B. Feldstein, 2012a: Mechanisms of Arctic surface air temperature change in response to the Madden–Julian oscillation. *J. Climate*, **25**, 5777–5790, https://doi.org/10.1175/JCLI-D-11-00566.1.

——, ——, and ——, 2012b: Arctic response to an MJO-like tropical heating in an idealized GCM. *J. Atmos. Sci.*, **69**, 2379–2393, https://doi.org/10.1175/JAS-D-11-0261.1.

Zhou, S., and A. J. Miller, 2005: The interaction of the Madden–Julian oscillation and the Arctic Oscillation. *J. Climate*, **18**, 143–159, https://doi.org/10.1175/JCLI3251.1.

——, M. L'Heureux, S. Weaver, and A. Kumar, 2012: A composite study of the MJO influence on the surface air temperature and precipitation over the continental United States. *Climate Dyn.*, **38**, 1459–1471, https://doi.org/10.1007/s00382-011-1001-9.